

# Stationary wave and surface radiative effects weaken and delay the near-surface response to stratospheric ozone depletion

Chaim I Garfinkel<sup>1</sup>, Ian White<sup>1</sup>, Edwin P Gerber<sup>2</sup>, Seok-Woo Son<sup>3</sup>, and Martin Jucker<sup>4</sup>

<sup>1</sup>Hebrew University of Jerusalem

<sup>2</sup>New York University

<sup>3</sup>Seoul National University

<sup>4</sup>University of New South Wales

November 22, 2022

## Abstract

An intermediate complexity moist General Circulation Model is used to investigate the factor(s) controlling the magnitude of the surface impact from Southern Hemisphere springtime ozone depletion. In contrast to previous idealized studies, a model with full radiation is used, which allows focus on the full range of feedbacks between incoming ultraviolet radiation and temperature variations. In addition, the model can be run with a varied representation of the surface, from a zonally uniform aquaplanet to a highly realistic configuration. The model captures the positive Southern Annular Mode response to ozone depletion evident in observations and comprehensive models in December through February. It is shown that while synoptic waves dominate the long-term poleward jet shift, the initial response includes changes in planetary waves which simultaneously moderate the polar cap cooling (i.e., a negative feedback), but also constitute nearly half of the initial momentum flux response that shifts the jet polewards. Enhanced ultraviolet absorption at the surface due to the ozone hole drives an additional negative feedback on the poleward jet shift. The net effect is that stationary waves and surface radiative effects weaken the circulation response to ozone depletion, and also delay the response until summer rather than spring when ozone depletion peaks.

1           **Stationary wave and surface radiative effects weaken and delay the**  
2                   **near-surface response to stratospheric ozone depletion**

3           Chaim I. Garfinkel,<sup>a</sup> Ian White,<sup>a</sup> Edwin P. Gerber,<sup>b</sup> Seok-Woo Son,<sup>c</sup> Martin Jucker,<sup>d</sup>

4           <sup>a</sup> *The Hebrew University of Jerusalem, Institute of Earth Sciences, Edmond J. Safra Campus,*  
5                                   *Givat Ram, Jerusalem, Israel*

6           <sup>b</sup> *Courant Institute of Mathematical Sciences, New York University, New York, USA*

7           <sup>c</sup> *School of Earth and Environmental Sciences, Seoul National University, Seoul, South Korea*

8           <sup>d</sup> *Climate Change Research Centre and ARC Centre of Excellence for Climate Extremes,*  
9                                   *University of New South Wales, Sydney, Australia*

10   *Corresponding author:* Chaim I. Garfinkel, The Hebrew University of Jerusalem, In-  
11   stitute of Earth Sciences, Edmond J. Safra Campus, Givat Ram, Jerusalem, Israel,  
12   chaim.garfinkel@mail.huji.ac.il.

13 ABSTRACT: An intermediate complexity moist General Circulation Model is used to investigate  
14 the factor(s) controlling the magnitude of the surface impact from Southern Hemisphere springtime  
15 ozone depletion. In contrast to previous idealized studies, a model with full radiation is used, which  
16 allows focus on the full range of feedbacks between incoming ultraviolet radiation and temperature  
17 variations. In addition, the model can be run with a varied representation of the surface, from a  
18 zonally uniform aquaplanet to a highly realistic configuration. The model captures the positive  
19 Southern Annular Mode response to ozone depletion evident in observations and comprehensive  
20 models in December through February. It is shown that while synoptic waves dominate the  
21 long-term poleward jet shift, the initial response includes changes in planetary waves which  
22 simultaneously moderate the polar cap cooling (i.e., a negative feedback), but also constitute nearly  
23 half of the initial momentum flux response that shifts the jet polewards. Enhanced ultraviolet  
24 absorption at the surface due to the ozone hole drives an additional negative feedback on the  
25 poleward jet shift. The net effect is that stationary waves and surface radiative effects weaken  
26 the circulation response to ozone depletion, and also delay the response until summer rather than  
27 spring when ozone depletion peaks.

## 28 **1. Introduction**

29 Antarctic springtime ozone concentrations decreased in the last few decades of the twentieth  
30 century due to anthropogenic emissions of chlorofluorocarbons (Solomon et al. 1986), and only  
31 recently have begun the slow process of recovery (Weber et al. 2018). Ozone depletion is known  
32 to have been the dominant contributor over the late 20th century to a poleward shift of the austral  
33 summer Southern Hemisphere (SH) tropospheric midlatitude jet, Southern Annular Mode (SAM),  
34 precipitation, and storm tracks, and to have led to an expansion of the summer Hadley Cell  
35 (Trenberth and Stepaniak 2002; Gillett and Thompson 2003; Son et al. 2010; Thompson et al.  
36 2011; Kang et al. 2011; Polvani et al. 2011; McLandress et al. 2011; Eyring et al. 2013; Gerber and  
37 Son 2014; Gonzalez et al. 2014; Previdi and Polvani 2014; Waugh et al. 2015; Seviour et al. 2017;  
38 Son et al. 2018). Over the next ~50 years, ozone recovery is expected to nearly cancel out changes in  
39 the tropospheric jet and Hadley Cell that would otherwise be forced by greenhouse gases (Son et al.  
40 2008; Polvani et al. 2011; Arblaster et al. 2011; Barnes and Polvani 2013; Gerber and Son 2014;  
41 Banerjee et al. 2020). Despite this clear evidence, the mechanism whereby ozone depletion leads  
42 to a downward impact, and the details of how this mechanism governs the magnitude of the impact,  
43 are still unclear, e.g. as noted in successive WMO Ozone assessments (World Meteorological  
44 Organization 2011, 2014; Karpechko et al. 2018).

45 This study focuses on two processes thought to be important for the downward impact: radiative  
46 effects and the role of planetary vs. synoptic waves. Radiative effects, and in particular reduced  
47 downward propagating longwave due to colder stratospheric temperatures, may be important for  
48 the tropospheric (Grise et al. 2009) and the surface temperature (Yang et al. 2014) response to  
49 ozone depletion. However as noted by Trenberth and Stepaniak (2002) and Previdi and Polvani  
50 (2014), the SAM accounts for around half of the observed surface warming over the Antarctic  
51 Peninsula, nearly all of the observed cooling over East Antarctica, and much of the warming over  
52 Patagonia. In addition, the longwave changes due to a colder stratosphere will be balanced in  
53 part by enhanced shortwave downwelling, as UV previously absorbed in the stratosphere can now  
54 reach the surface (Chiodo et al. 2017). Regardless of how the tropospheric cooling arises, the role  
55 of this tropospheric cooling for the jet shift, as compared to other mechanisms for the downward  
56 impact, has not been thoroughly explored in previous work though Chiodo et al. (2017) found the  
57 net radiative effect to be weak.

58 SH stationary waves are dominated by wave-1, even in the troposphere (Garfinkel et al. 2020a),  
59 and while SH stationary waves are weaker than their counterparts in the Northern Hemisphere,  
60 they contribute roughly half of the heat flux in spring in the lower stratosphere (Kållberg et al.  
61 2005) and contribute to the inter-model spread in the timing of the ozone-hole breakup (Hurwitz  
62 et al. 2010). A commonly used model in studies focusing on the mechanism(s) for the surface  
63 response to ozone depletion is a dry dynamical core with a flat bottom (e.g. Kushner and Polvani  
64 2004; Sun et al. 2014; Yang et al. 2015; Smith and Scott 2016) allowing for transient planetary  
65 waves only, or a highly idealized mountain (Gerber and Polvani 2009; Domeisen et al. 2013). The  
66 importance of stationary waves in the SH for a surface response cannot be readily evaluated in such  
67 setups by construction. Many of these studies using flat-bottomed models nevertheless conclude  
68 that planetary waves are crucial for the surface response. For example, Smith and Scott (2016)  
69 find that the response to a stratospheric perturbation is weaker if interactions between planetary-  
70 and synoptic-scale waves are suppressed, while Domeisen et al. (2013) find that the jet shifts in  
71 the opposite direction if only planetary waves are present, ruling out the possibility that the jet  
72 shift occurs purely as a response to changes in the planetary- or synoptic-scale wave fields alone.  
73 However the lack of stationary planetary waves in these models resembling those in the SH may  
74 lead to a mis-representation of the total impact of planetary waves.

75 The goals of this study are to answer these two questions:

- 76 1. how do changes in UV absorption at the surface (due to the lack of absorption in the strato-  
77 sphere) affect the timing and intensity of the jet shift?
- 78 2. what is the relative role of synoptic vs. planetary waves for the downward impact?

79 We take advantage of a recently developed intermediate complexity model that can delineate the  
80 role of these two effects. First, it can be run alternately with realistic stationary waves or without any  
81 zonal asymmetry in the bottom boundary (e.g., topography), and thus clarify the role of stationary  
82 waves for the surface response. Second, it can be run alternately with an ozone hole in which  
83 surface shortwave feedbacks are present, or with a stratospheric diabatic temperature tendency that  
84 mimics the shortwave effects of ozone depletion in the stratosphere only, thus clarifying the role  
85 of surface shortwave changes.

86 After introducing this model in Section 2 and our diagnostics in Section 3, we demonstrate  
87 in Section 4 that the model in its most realistic configuration simulates a quantitatively realistic

88 response to ozone depletion, but that the response is significantly stronger in an aquaplanet config-  
89 uration. We consider two complementary reasons for this effect in Section 5, and then summarize  
90 our results and place them in the context of previous work in Section 6.

## 91 **2. A model of an idealized moist atmosphere (MiMA)**

92 We use the Model of an idealized Moist Atmosphere (MiMA) introduced by Jucker and Gerber  
93 (2017), Garfinkel et al. (2020b), and Garfinkel et al. (2020a). This model builds on the aquaplanet  
94 models of Frierson et al. (2006), Frierson et al. (2007), and Merlis et al. (2013). Very briefly,  
95 the model solves the moist primitive equations on the sphere, employing a simplified Betts-Miller  
96 convection scheme (Betts 1986; Betts and Miller 1986), idealized boundary layer scheme based  
97 on Monin-Obukhov similarity theory, and a purely thermodynamic (or slab) ocean. An important  
98 feature for this paper is that we use a realistic radiation scheme Rapid Radiative Transfer Model  
99 (RRTMG) (Mlawer et al. 1997; Iacono et al. 2000), which allows us to explicitly simulate the  
100 radiative response to ozone depletion, unlike previous studies using more idealized models with  
101 Newtonian cooling. Please see Jucker and Gerber (2017) for more details.

102 This model can be run alternately as an aquaplanet, or with stationary waves quantitatively similar  
103 to those in comprehensive models (Garfinkel et al. 2020b,a). The most realistic configuration of  
104 MiMA used in this study has boundary forcings that are identical to those of Garfinkel et al.  
105 (2020a), and this configuration is referred to as STAT in the rest of this paper. MiMA has no  
106 true land, rather the properties of the surface at gridpoints that are land on Earth are modified to  
107 mimic land (Figure 3 of Jucker and Gerber 2017). The net effect is that the STAT configuration  
108 includes three sources of zonal asymmetry in the lower boundary: orography, prescribed east-west  
109 ocean heat transport, and land-sea contrast (i.e., difference in heat capacity, surface friction, and  
110 moisture availability between “ocean” gridpoints and “land” gridpoints). The specifications of  
111 these forcings can be found in Garfinkel et al. (2020a). Note that the same albedo value is applied  
112 to all wavelengths of incoming solar radiation.

113 We analyze the response to an identical ozone hole for four different tropospheric configura-  
114 tions: (i) the Southern Hemisphere (SH) of STAT, (ii) the Northern Hemisphere (NH) of STAT  
115 (STATNH), (iii) an aquaplanet with albedo of 0.27 globally (including over “Antarctica”), and (iv)  
116 and an aquaplanet but in which the albedo over “Antarctica” is increased to 0.8 and elsewhere

117 lowered to 0.23 (as in STAT, see equation A3 of Garfinkel et al. 2020a) to help maintain a similar  
 118 global mean temperature. We refer to these last two experiments as AQUA27 and AQUA80 in  
 119 the rest of this paper. The AQUA runs have no stationary waves, but both aquaplanet integrations  
 120 still include north-south ocean heat transport (Eq. A4 of Garfinkel et al. 2020a). The aquaplanet  
 121 runs use a mixed-layer depth of 75m everywhere, in contrast to STAT which has a mixed layer  
 122 depth of 2.5m over "land" and a varying depth for ocean gridpoints (see Eq. A2 of Garfinkel et al.  
 123 2020a). The NH STAT configuration is not meant to simulate a boreal winter ozone "hole", either  
 124 as observed in 1997, 2011 or 2020 (Hurwitz et al. 2011; Manney et al. 2011; Rao and Garfinkel  
 125 2020; Lawrence et al. 2020; Rao and Garfinkel 2021) or as in a world avoided scenario (Newman  
 126 et al. 2009; Garcia et al. 2012). Rather, it explores how the exact same change of ozone impacts  
 127 the circulation with a very different climatology of stationary (and synoptic) waves.

128 For all tropospheric configurations, we compare a pair of simulations: (1) a preindustrial sim-  
 129 ulation forced with the monthly varying climatology of ozone in the CMIP6 ozone specification  
 130 averaged from 1860 to 1899 (PI simulation; Checa-Garcia et al. 2018; Checa-Garcia 2018); and  
 131 (2) a simulation forced with the monthly varying climatology of ozone in the CMIP6 ozone speci-  
 132 fication averaged from 1990 to 1999, which we then further reduce by a factor of 4 between 150hPa  
 133 and 30hPa and poleward of 65S following:

$$\Phi(\varphi) = 1 - 3/8 \left( 1 - \tanh \left[ \frac{\varphi + 65^\circ}{3^\circ} \right] \right), \quad (1)$$

134 where  $\varphi$  denotes latitude (ozone hole simulation). This additional reduction in the polar lower  
 135 stratosphere is intended to capture springs with stronger than average ozone depletion (Previdi and  
 136 Polvani 2014), and is included to enhance the signal to noise ratio. An experiment without this  
 137 additional reduction leads to a weaker surface response, which is consistent with previous work  
 138 that has argued that interannual variability of ozone concentrations can be used to improve the skill  
 139 of seasonal and subseasonal forecasting (Son et al. 2013; Bandoro et al. 2014; Hendon et al. 2020;  
 140 Jucker and Goyal 2021). The linearity of the response is discussed in more detail in Section 5c.

141 The ozone hole runs branch from October 1st of the last 65 years of the respective preindustrial  
 142 control runs, and are then integrated for at least 150 days. The results are shown in terms of the  
 143 difference between the ozone hole simulation and the PI simulation (ozone hole - PI), though all  
 144 conclusions are just as applicable to ozone recovery. The net effect on ozone is shown in Figure

145 1abc, which show days 1 to 30 (October), 31 to 70 (November and early December), and 71 to  
146 120 (rest of December and January). The ozone perturbation is evident throughout the spring and  
147 decays in early summer. In the polar lower stratosphere, more than 90% of the preindustrial ozone  
148 is locally depleted, and this reduction is within the range of realistic values (Solomon et al. 2005;  
149 Previdi and Polvani 2014). Ozone actually increases slightly in the upper stratosphere in summer  
150 due to dynamical feedbacks (Stolarski et al. 2006).

151 In order to isolate the role of surface shortwave absorption, and also to more cleanly connect  
152 our results to studies using dry models with an imposed diabatic heating (Kushner and Polvani  
153 2004; Sheshadri and Plumb 2016; White et al. 2020), we also performed simulations in which  
154 a diabatic heating perturbation is imposed in the lower stratosphere. Our goal is to match the  
155 stratospheric diabatic heating perturbation due to ozone, and thus we show in Figure 1d-f the  
156 diabatic heating perturbation due to the reduced ozone as computed by the model. The diabatic  
157 heating rate is  $\sim -0.5\text{K/day}$  in the polar lower stratosphere. The upper stratospheric diabatic  
158 tendency is due to the dynamically induced warming resulting in enhanced longwave emission  
159 (Manzini et al. 2003; McLandress et al. 2010; Orr et al. 2012a). Motivated by this, we impose a  
160 diabatic perturbation between 150hPa and 30hPa of the form of equation 1, and hold it constant  
161 in time with no seasonality. The effect of this diabatic heating perturbation is explored both for a  
162 diabatic heating perturbation similar in magnitude and location to the one due to ozone depletion  
163 (peaking at  $-0.5\text{K/day}$ ; DIAB simulation) and also a factor of five larger (peaking at  $-2.5\text{K/day}$ ;  
164 DIAB5x simulation).

165 Table 1 summarizes all experiments included in this paper. For all integrations, the model is  
166 forced with  $\text{CO}_2$  concentrations fixed at 390ppmv and seasonally varying solar insolation. All  
167 simulations in this paper were run with a triangular truncation at wavenumber 42 (T42) with 40  
168 vertical levels.

### 174 3. Diagnostics

175 The role of synoptic and planetary waves in driving the poleward jet shift is diagnosed using the  
176 Eulerian mean zonal momentum budget:

169 TABLE 1. MiMA Experiments, with “Y” indicating a forcing is on and “N” indicating a forcing is off. For  
 170 ozone, we compare a “preindustrial” simulation using ozone concentrations from the CMIP6 read-in file over  
 171 the years 1860-1899 to a simulation using ozone concentrations from the CMIP6 read-in file over the years  
 172 1990-1999, which were then modified in the Antarctic lower stratosphere (see section 2) to capture a deeper  
 173 ozone hole evident in some years. The jet latitude is included for November in the SH.

Table: MiMA Model experiments

	surface zonal structure	“Antarctica” albedo	“Antarctica” mixed layer	Nov jet latitude
STAT, hole-PI	Y	0.8	2.5m	50.1S
AQUA80, hole-PI	N	0.8	75m	46.5S
AQUA27, hole-PI	N	0.27	75m	43.1S
STATNH, hole-PI	Y	0.8	2.5m	
STAT, diab-PI	Y	0.8	2.5m	50.1S
AQUA80, diab-PI	N	0.8	75m	46.5S
STAT, diab5x-PI	Y	0.8	2.5m	50.1S
AQUA80, diab5x-PI	N	0.8	75m	46.5S

$$\begin{aligned}
 \frac{\partial \bar{u}}{\partial t} = & - \underbrace{\left( \frac{1}{a \cos^2 \varphi} \frac{\partial}{\partial \varphi} (\cos^2 \varphi \overline{u'v'}_{k \leq 3}) + \frac{1}{\rho_0} \frac{\partial}{\partial z} (\rho_0 \overline{u'w'}_{k \leq 3}) \right)}_{eddy_{1-3}} \\
 & - \underbrace{\left( \frac{1}{a \cos^2 \varphi} \frac{\partial}{\partial \varphi} (\cos^2 \varphi \overline{u'v'}_{k > 3}) + \frac{1}{\rho_0} \frac{\partial}{\partial z} (\rho_0 \overline{u'w'}_{k > 3}) \right)}_{eddy_{4+}} \\
 & + \underbrace{f\bar{v}}_{fv} - \underbrace{\left( \bar{w} \frac{\partial \bar{u}}{\partial z} + \frac{\bar{v}}{a \cos \varphi} \frac{\partial}{\partial \varphi} (\bar{u} \cos \varphi) \right)}_{advect} + \bar{X} + \text{res} \quad (2)
 \end{aligned}$$

177 (e.g., Andrews et al. 1987; Hitchcock and Simpson 2016) where the acceleration of the zonal-mean  
 178 zonal wind on the left hand side is contributed to by processes associated with (from left to right  
 179 on the right hand side): eddy momentum flux convergence due to planetary waves ( $eddy_{1-3}$ ),  
 180 eddy momentum flux convergence due to synoptic waves ( $eddy_{4+}$ ), Coriolis torques acting on the  
 181 meridional motion ( $f\bar{v}$ ), mean flow momentum advection (advect), and parameterised processes  
 182 including the zonal wind tendency due to vertical and horizontal diffusion and gravity-wave drag  
 183 in the model ( $\bar{X}$ ). All variables follow standard notation (e.g., see Andrews et al. 1987). The

184 final term (res) is the budget residual and is contributed to by issues associated with sampling and  
185 truncation errors.

186 The Southern Annular mode (SAM) and the e-folding timescale of the corresponding principle  
187 component timeseries is computed following the methodology of Baldwin et al. (2003) and Gerber  
188 et al. (2008). Jet latitude is computed by fitting the 850hPa zonal mean zonal wind near the  
189 jet maxima (as computed at the model's T42 resolution) to a second order polynomial, and then  
190 evaluating the polynomial at a meridional resolution of  $0.12^\circ$ . The latitude of the maximum of this  
191 polynomial is the jet latitude (Garfinkel et al. 2013a).

#### 192 **4. The response to an identical ozone perturbation in STAT and in AQUA80**

193 We begin by showing that in the STAT configuration of MiMA, ozone loss leads to impacts  
194 similar to those shown in previous works using reanalysis or comprehensive models. Figure 1ghi  
195 shows the temperature response to reduced ozone. Temperatures in the polar lower stratosphere  
196 gradually decrease over the first two months and reach -15K by November, and the anomaly  
197 propagates downward to near the tropopause in late December (Figure 1i). This cooling is similar  
198 to that observed during years with a particularly strong ozone hole relative to 1960s conditions  
199 (Randel et al. 2009; Previdi and Polvani 2014). The zonal wind response is shown in Figure  
200 1jkl, and captures the response evident in reanalysis, CMIP, and CCM data (Previdi and Polvani  
201 2014; Son et al. 2018). Changes in 500hPa geopotential height also resemble the canonical SAM  
202 pattern (Figure 2bc, Kidson 1988; Thompson and Wallace 2000; Thompson et al. 2011) with lower  
203 heights in subpolar latitudes and higher heights between 40S and 50S. The model also simulates the  
204 precipitation response to ozone depletion (unlike dry models used in many mechanistic studies).  
205 Figure 2def shows an increase in precipitation over Southeastern Australia and Southeastern South  
206 America and drying over New Zealand (in agreement with observed trends; Hendon et al. 2007;  
207 Ummenhofer et al. 2009; Gonzalez et al. 2014).

208 The increase in subpolar zonal wind peaks near day 90 at 70hPa (January 1st; Figure 3a), though  
209 higher in the stratosphere the response peaks earlier, and is followed by a zonal wind and SAM  
210 response in the troposphere (Figure 3b for 850hPa wind and 3c for geopotential height). While a  
211 tropospheric response begins to develop in November, the response peaks in January and persists  
212 into February in agreement with previous work.

213 Encouraged by the quantitative accuracy of the response in the most realistic configuration,  
214 we now take advantage of the flexibility of the idealized model in order to understand the role  
215 of stationary waves and shortwave effects for the surface response. As discussed in Section  
216 2, the same ozone perturbation has also been imposed in two aquaplanet configurations of the  
217 model (differing only in the polar albedo) and in the Northern Hemisphere. We begin with  
218 the aquaplanet configuration with a polar albedo of 0.8 (AQUA80), as this turns out to be the  
219 tropospheric configuration with the largest surface response to ozone depletion. Even though the  
220 ozone perturbations are identical, the wind response (Figure 1, bottom row) is larger in AQUA80.  
221 The difference in zonal wind response between the two configurations is statistically significant at  
222 the 5% level after day 45 in both the stratosphere and troposphere (Figure 4). The geopotential  
223 height response in the troposphere is more than twice as large in AQUA80 than in STAT (Figure  
224 2abc vs 5abc and Figure 3c vs. 6c), and the precipitation response is also stronger although  
225 less regionally focused due to the lack of Antarctica orography (Figure 5def). The difference in  
226 response is evident both in November and in December/January (Figure 6b and Figure 7abc).

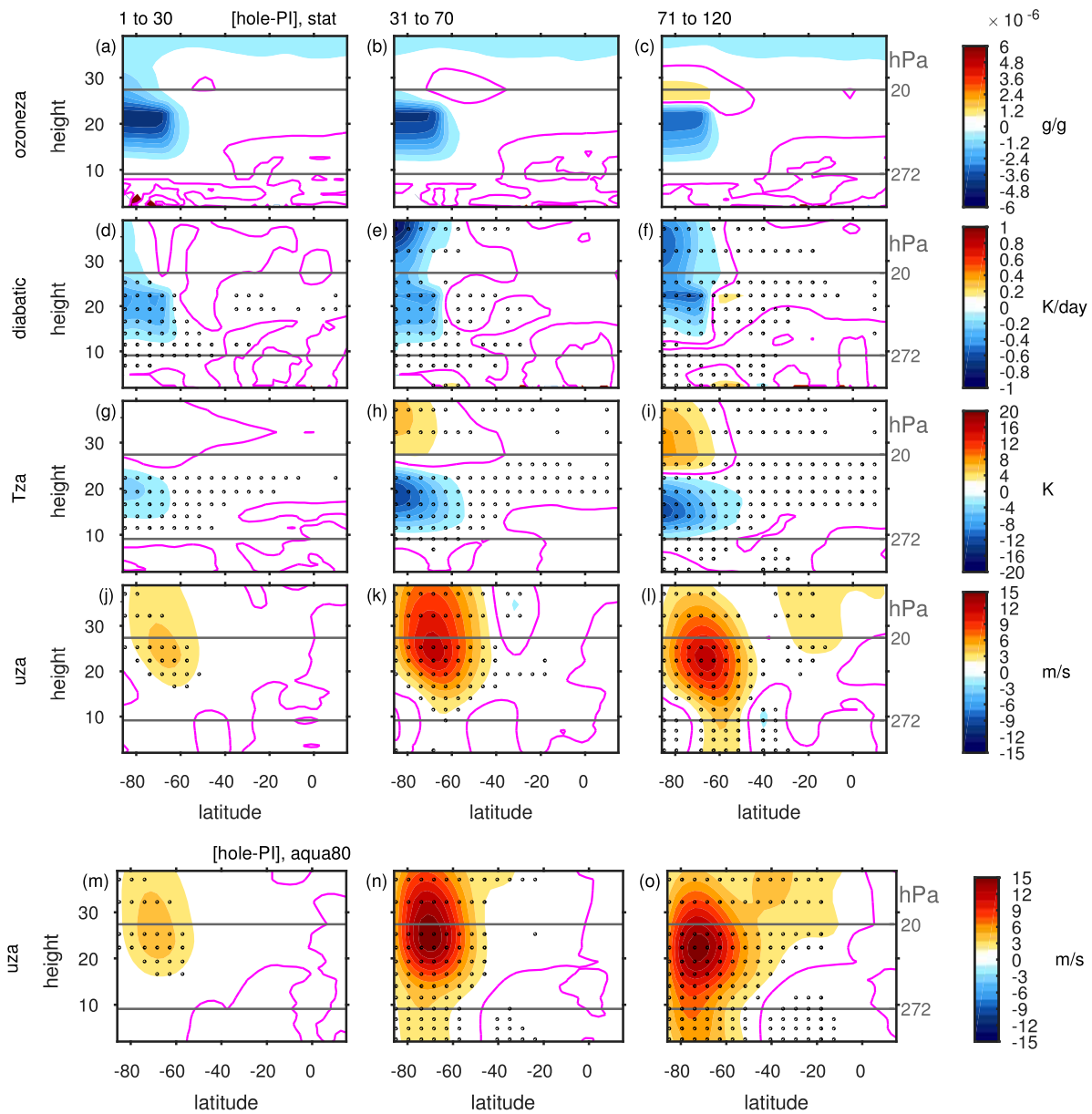
## 256 **5. Why the stronger response for AQUA80?**

257 STAT and AQUA80 differ in two aspects: AQUA80 has a mixed layer depth of 75m over  
258 Antarctica while STAT has a mixed layer depth of only 2.5m. Even though both configurations  
259 have an albedo of 0.8 over Antarctica, this difference in the mixed-layer depth leads to a polar  
260 surface warming in STAT of nearly 1K<sup>1</sup>, but a 4K cooling occurs in AQUA80 consistent with  
261 dynamically induced colder temperatures associated with a positive SAM (Figure 7d and contrast  
262 Figure 5ghi and 2ghi). The warming in STAT extends from the surface into the mid-troposphere  
263 (Figure 8b) and the difference between STAT and AQUA80 is statistically significant (Figure 8c).  
264 Section 5a isolates the impact of this surface shortwave response for the circulation response.

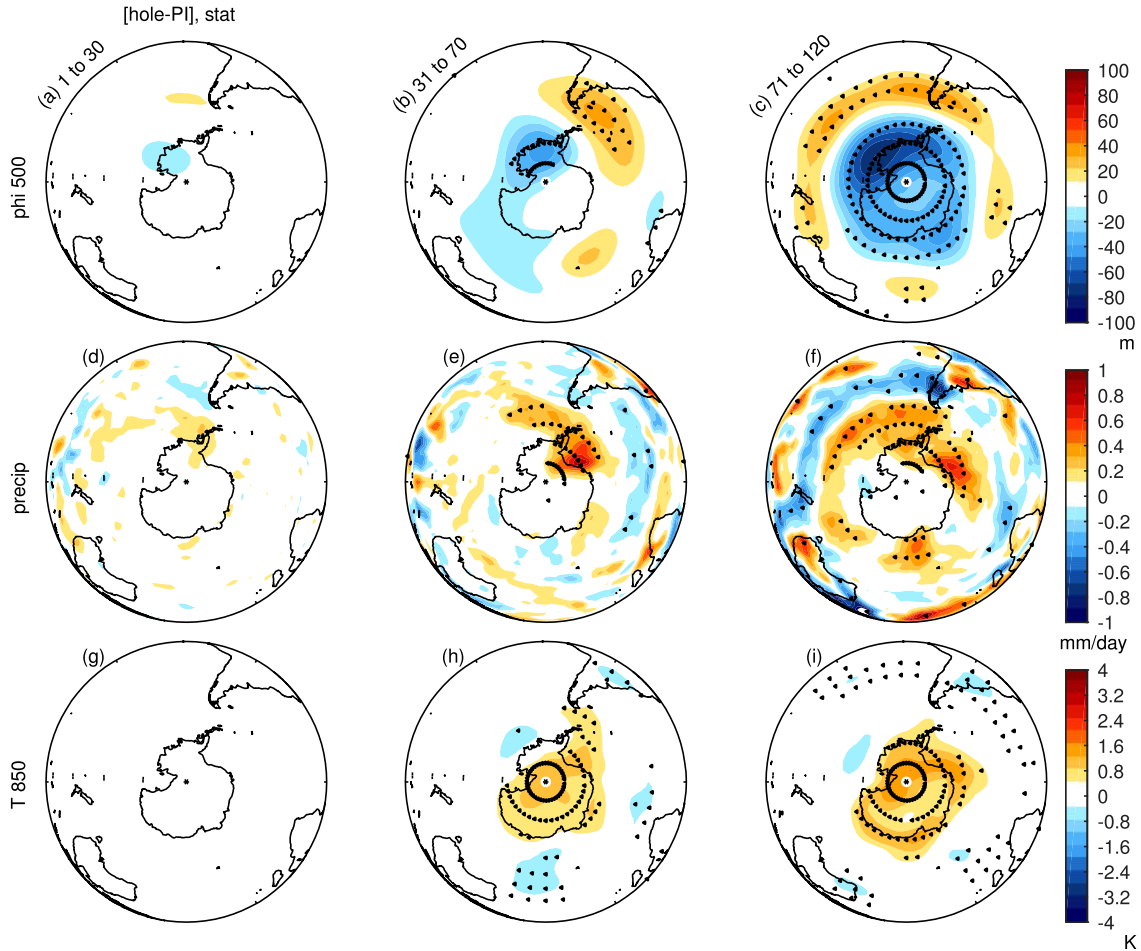
265 These integrations also differ in their representation of stationary waves: AQUA80 clearly has  
266 none. Section 5b considers the impact of stationary waves for the response.

---

<sup>1</sup>Note that observations indicate a cooling over Antarctica, a feature STAT misses, likely because our albedo is identical for visible/UV and near-IR, while in reality the albedo is approximately 0.97 for visible/UV but much lower for near-IR (Wiscombe and Warren 1980; Grenfell et al. 1994; Gardner and Sharp 2010; Chiodo et al. 2017).



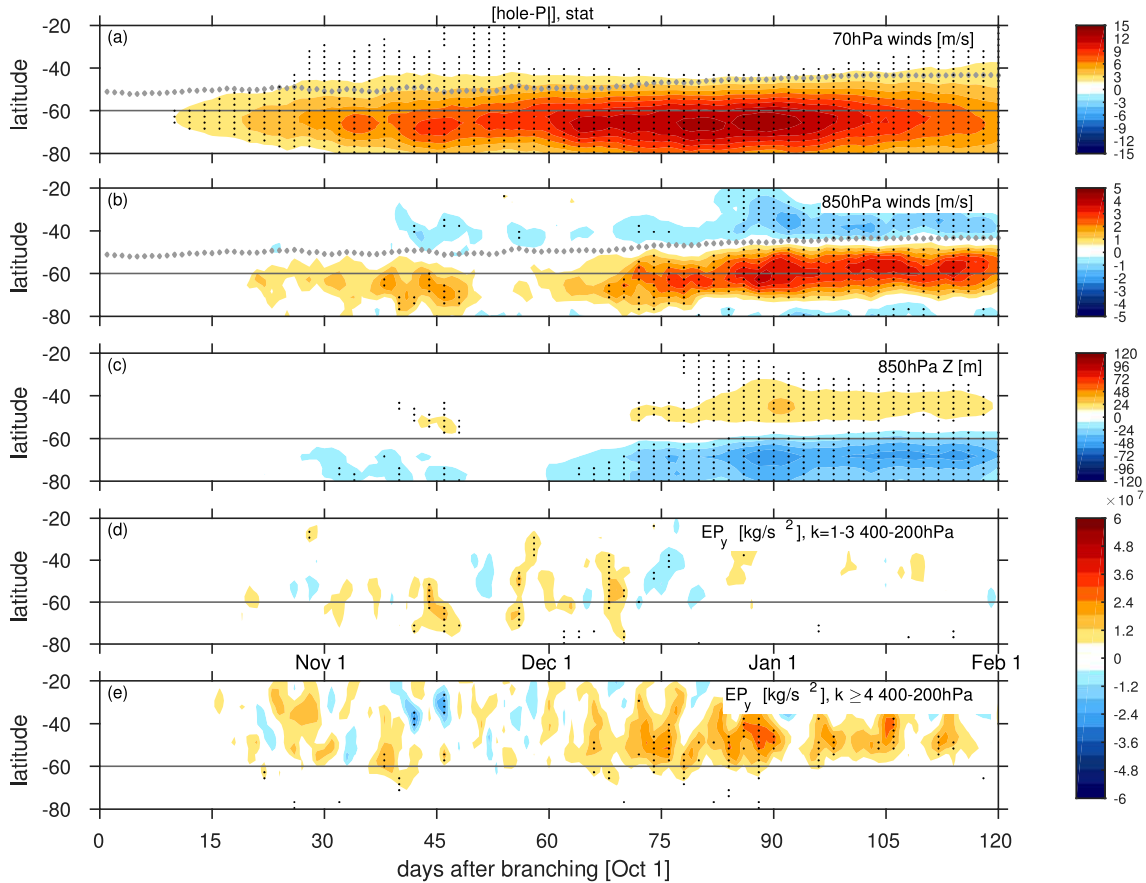
227 FIG. 1. Zonal-mean responses to ozone loss [i.e., ozone hole minus preindustrial (PI)] in the most realistic  
 228 configuration, STAT, in (left) days 1-30 after branching, i.e. October; (middle) days 31 to 70, i.e. November and  
 229 December 1-10; (right) days 71 to 120, i.e. December 11 through January 30. (a-c) ozone perturbation; (d-f)  
 230 diabatic heating rate computed as the sum of the temperature tendency due to longwave, shortwave, and latent  
 231 heat release; (g-i) temperature; (j-l) zonal wind. The bottom row is as in (j) through (l) but for an aquaplanet  
 232 configuration with “Antarctic” albedo=0.8. Stippling indicates anomalies statistically significant at the 95% level.  
 233 The zero contour is shown in magenta.



234 FIG. 2. Map view of ozone loss response (ozone hole - PI) in the most realistic configuration in (left) days  
 235 1-30 after branching, i.e. October; (middle) days 31 to 70; (right) days 71 to 120. (a-c) geopotential height at  
 236 500hPa; (d-f) precipitation; (g-i) temperature at 850hPa. Stippling indicates anomalies statistically significant at  
 237 the 95% level.

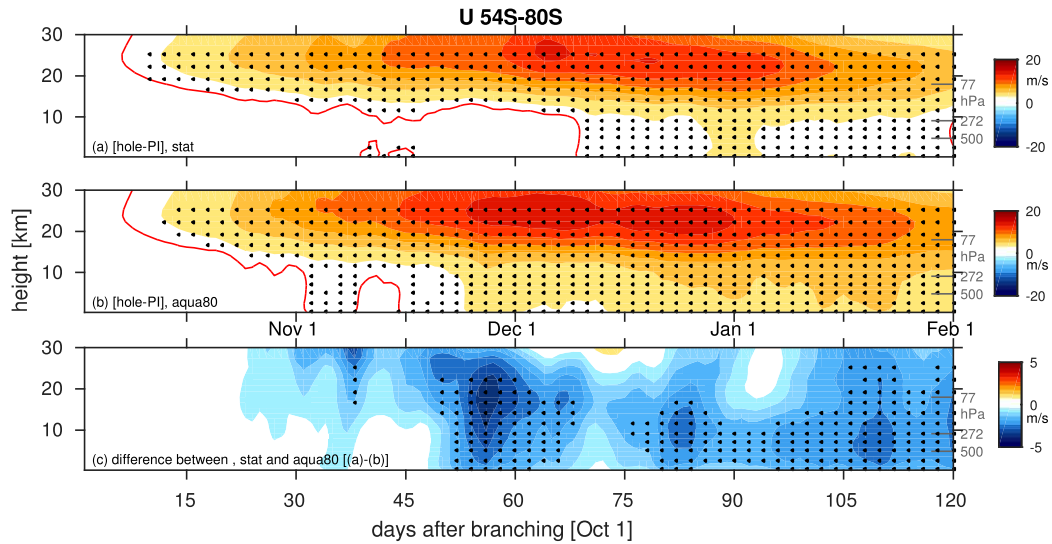
267 *a. A shortwave negative feedback for the jet response*

268 As discussed above, the near-surface of Antarctica warms for STAT and cools for AQUA80  
 269 due to differences in surface processes (Figure 8c). An ozone hole allows more UV to reach  
 270 the surface, and in STAT a warmer near-surface tropospheric polar cap leads to higher heights  
 271 throughout the column, including at 500hPa (Figure 5abc and 2abc) and above. The net effect is  
 272 that the meridional gradient in geopotential is more extreme in AQUA80 than in STAT, and the  
 273 jet shift is therefore stronger. The hypsometric equation can be used to quantify the contribution  
 274 of changes in temperature below 500hPa versus those above 500hPa for changes in stratospheric



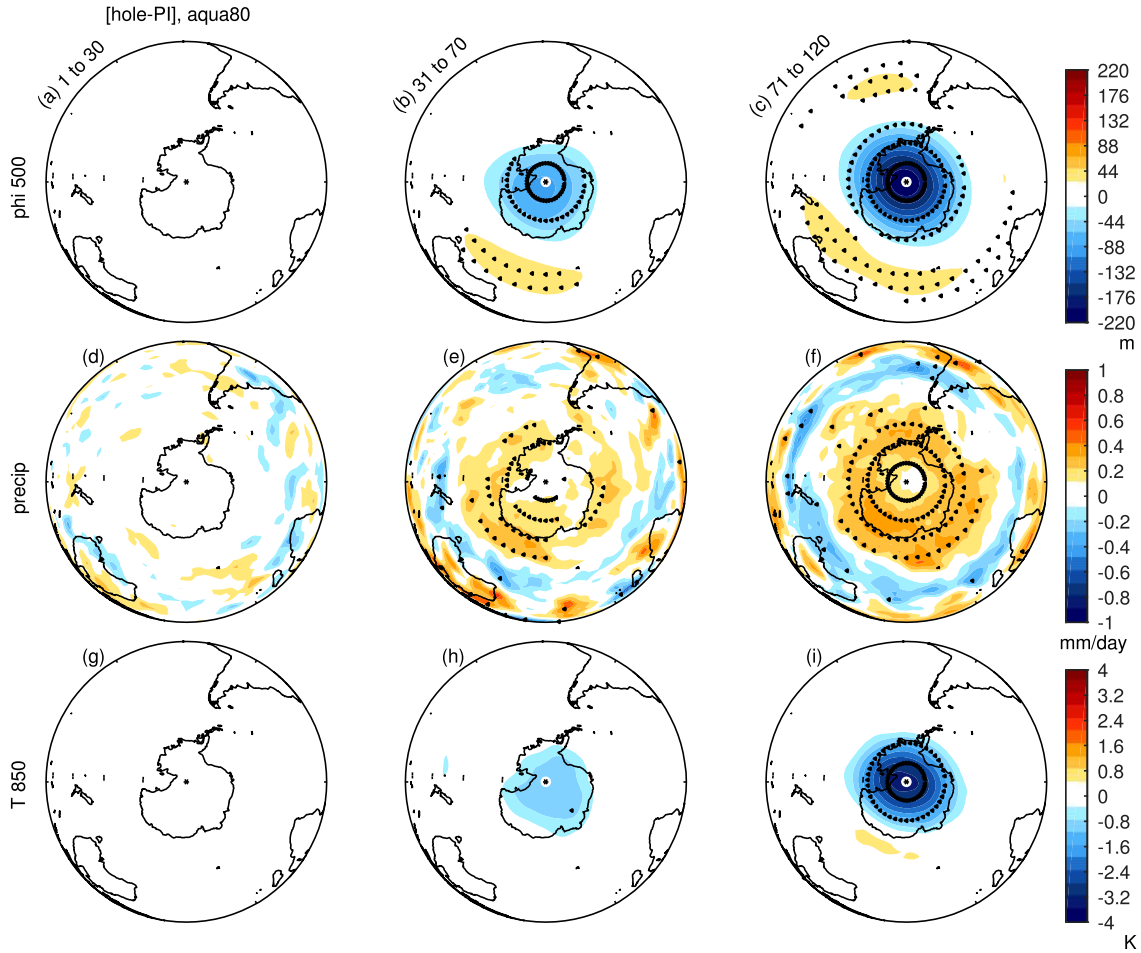
238 FIG. 3. Development and downward propagation of the response to the ozone perturbation in the most realistic  
 239 configuration. (a) 70hPa zonal wind; (b) 850hPa zonal wind; (c) 850hPa polar cap geopotential height; upper  
 240 tropospheric meridional Eliassen-Palm flux due to (d) planetary and (e) synoptic waves. The tropospheric jet  
 241 latitude is shown in (a) and (b) with gray diamonds. Stippling indicates anomalies statistically significant at the  
 242 95% level.

275 polar cap height (and therefore subpolar zonal wind). Even in the lower stratosphere approximately  
 276 30% of the difference in polar cap height between STAT and AQUA80 is due to changes in lower  
 277 tropospheric temperature. The net effect is that the polar surface warming in STAT in isolation  
 278 would lead to an equatorward jet shift which cancels part of the ozone-induced poleward shift, and  
 279 hence is a negative feedback. Conversely, a polar cap cooling due to e.g., longwave effects can  
 280 help drive a poleward shift (consistent with Grise et al. 2009). However, in our STAT simulation  
 281 this longwave effect is weaker than the shortwave effect.



243 FIG. 4. Evolution of zonal wind from 54S to 80S for the [ozone hole-PI] runs with (a) realistic stationary  
 244 waves, (b) an aquaplanet, with “Antarctic” albedo equal to 0.8. (c) difference between (a) and (b). The contour  
 245 interval is 2m/s in (a) and (b) and 0.5m/s in (c). The 1m/s contour is indicated in red in (a) and (b). Stippling  
 246 indicates anomalies statistically significant at the 95% level.

282 The comparison of STAT to AQUA80 includes both this shortwave effect and also the stationary  
 283 wave effect to be discussed shortly, and in order to isolate the surface shortwave effect, we perform  
 284 an additional aquaplanet integration with polar albedo of 0.27 (AQUA27). AQUA80 and AQUA27  
 285 differ only in the specification of albedo, and hence by comparing them we can focus on the effects  
 286 of shortwave radiation reaching the surface. In AQUA27, surface temperatures rise over Antarctica  
 287 (Figure 7d) due to enhanced ultraviolet absorption, opposite to AQUA80. The stratospheric zonal  
 288 wind response is weaker (Figure 7b and Figure 9), and consistent with a weaker stratospheric  
 289 response and with lower tropospheric warming, the tropospheric wind response is weaker in  
 290 AQUA27 than in AQUA80 (Figure 7c, and Figure 9). This weakening of the response in AQUA27  
 291 vs. AQUA80 occurs even as the jet latitude is further equatorward and the e-folding timescale of  
 292 the SAM is slightly larger in AQUA27 (Figure 7, Table 1), two factors which would be expected to  
 293 lead to a stronger response (Garfinkel et al. 2013b).



247 FIG. 5. As in Figure 2 but for an aquaplanet configuration with “Antarctic” albedo=0.8. Note that the color  
 248 scale for the top row differs from Figure 2.

307 *b. A stationary wave negative feedback for the jet response*

308 In addition to this surface shortwave effect, there is an additional cause for the differences between  
 309 AQUA80 and STAT in the intensity of the ozone-induced jet shift. Adding stationary waves leads  
 310 to less of a cooling of the polar lowermost stratosphere (Figure 7a and Figure 8c) even though the  
 311 ozone perturbation is identical. This difference in response to an identical ozone perturbation occurs  
 312 because the strengthened vortex in late fall and early summer due to ozone depletion favors more  
 313 upward wave propagation, and the subsequent enhanced wave convergence within the stratosphere  
 314 leads to dynamical warming of the polar cap via downwelling of the transformed Eulerian mean  
 315 vertical wind. This cancels a part of the radiatively driven cooling near the tropopause (not shown,

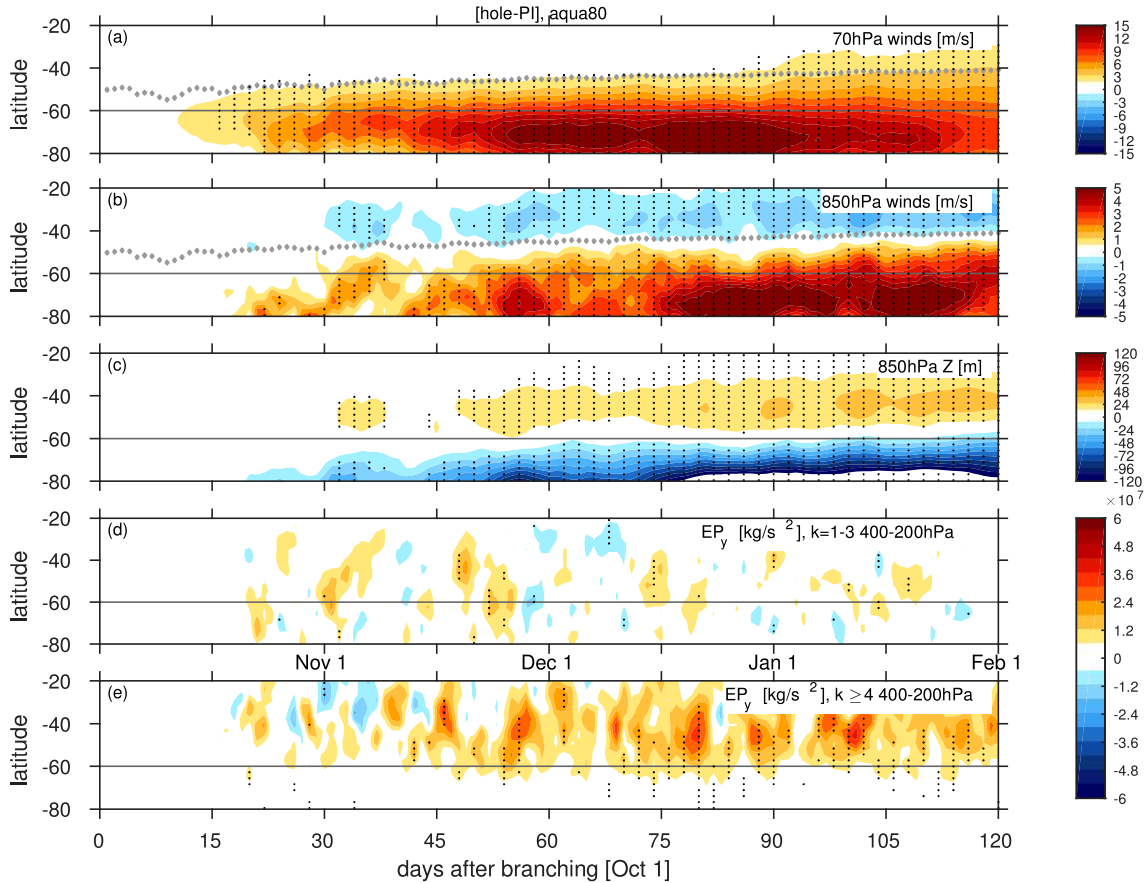
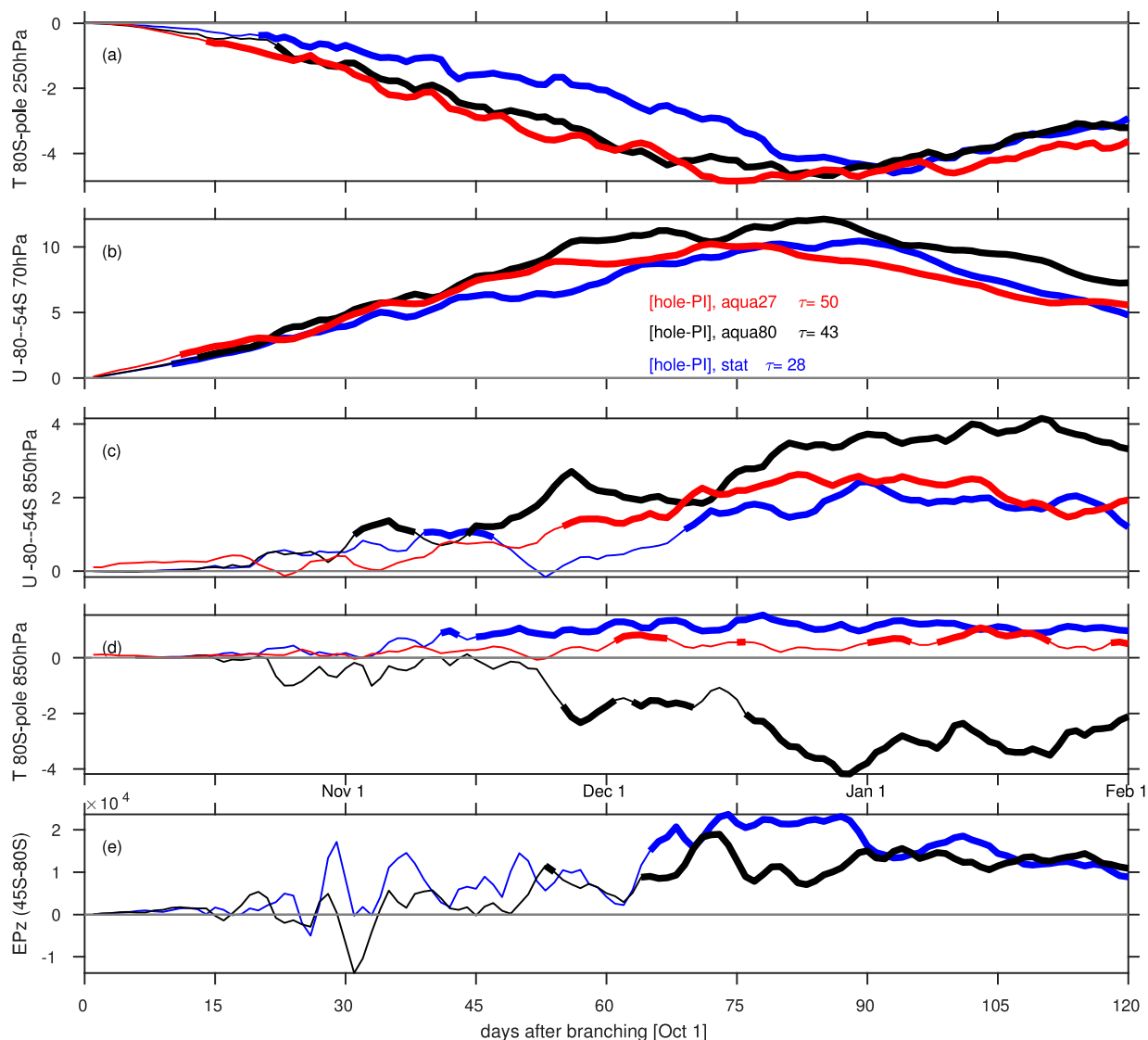
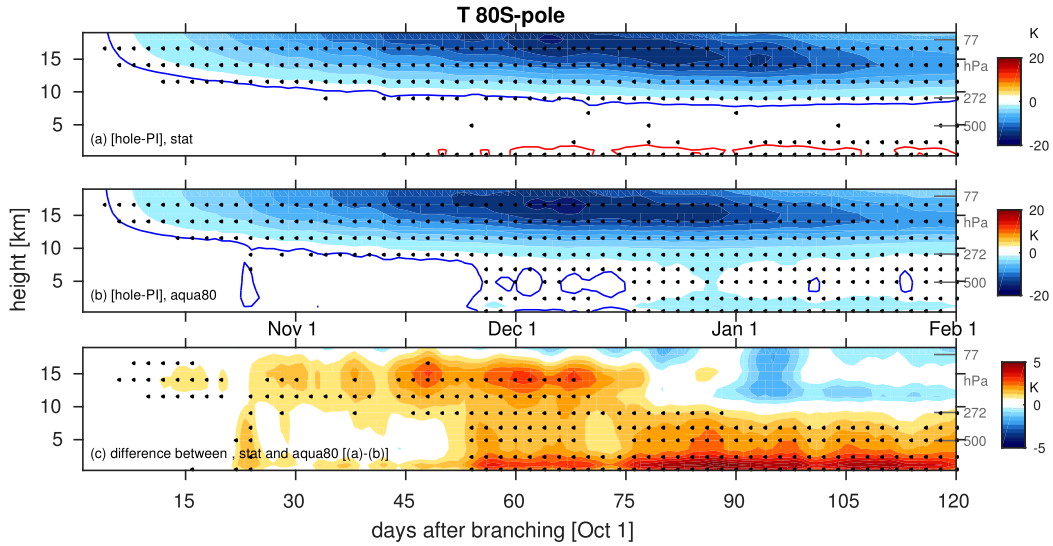


FIG. 6. As in Figure 3 but for aquaplanet with “Antarctic” albedo=0.8.

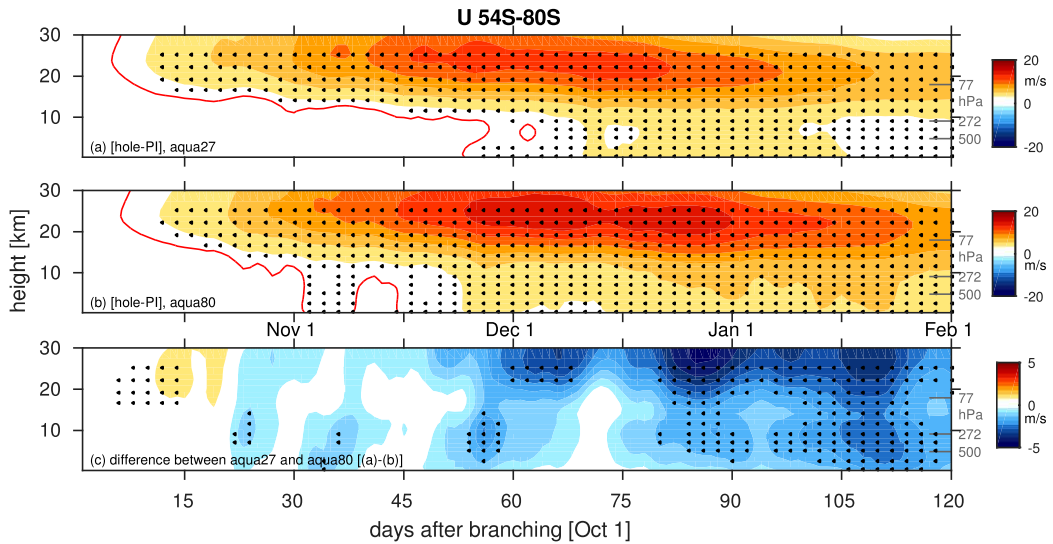
316 but as in Manzini et al. 2003; Li et al. 2010; McLandress et al. 2010; Orr et al. 2012a). However this  
 317 increase in upward propagating waves is more dramatic in the presence of stronger wave forcing  
 318 from below, and in STAT these upward propagating waves are indeed stronger due to the presence  
 319 of stationary waves. We demonstrate this effect in Figure 7e, which shows the vertical component  
 320 of the Eliassen-Palm flux at 40hPa, though other levels in the mid- and lower- stratosphere show a  
 321 similar response. In STAT, an ozone hole leads to increased upward wave flux by late October, and  
 322 the anomaly stays positive throughout the duration of the run. The increase in AQUA80 is weaker  
 323 however, and the difference between STAT and AQUA80 is statistically significant between days  
 324 75 and 90. The net effect is a warmer polar stratosphere in STAT (Figure 8c). Hence, stationary  
 325 waves act as a negative feedback on the surface and stratospheric response to ozone, acting to  
 326 partially offset the ozone-induced cooling and poleward jet shift.



249 FIG. 7. Summary of responses to ozone depletion [ozone hole-PI]. (a) polar cap temperature at 250hPa [K];  
 250 area-weighted average of zonal wind from 80S to 55S [m/s] at (b) 70hPa and (c) 850hPa; (d) polar cap temperature  
 251 at 850hPa [K]; (e) vertical component of the EP flux at 40hPa area-weighted average from 80S to 45S [ $kg/s^2$ ].  
 252 Blue line is for most realistic configuration. Red line is for an aquaplanet, with “Antarctic” albedo equal to 0.27.  
 253 Black line is for an aquaplanet, with “Antarctic” albedo equal to 0.8. A thick line indicates regions in which  
 254 a null hypothesis of no effect can be rejected at the 95% confidence level. The legend also includes the SAM  
 255 e-folding timescale of each configuration in January.

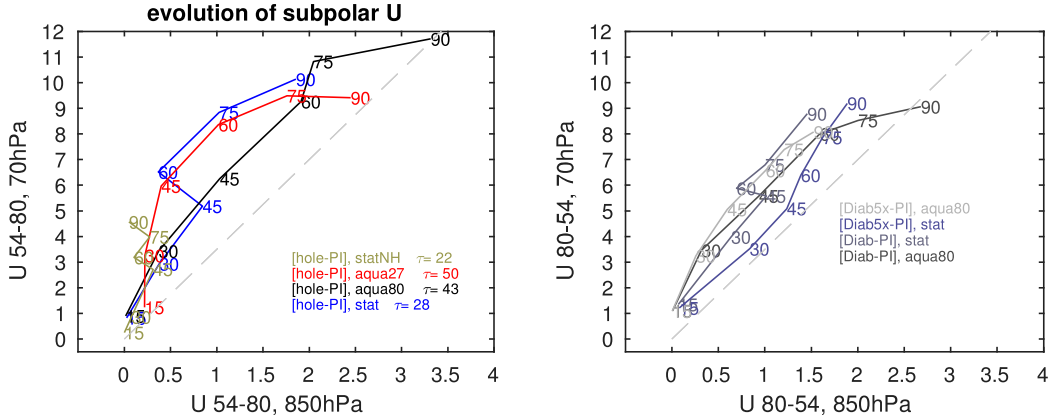


294 FIG. 8. Evolution of polar cap T for the [ozone hole-PI] runs with (a) realistic stationary waves, (b) an  
 295 aquaplanet, with “Antarctic” albedo equal to 0.8. (c) difference between (a) and (b). The -1K(1K) contour is  
 296 indicated in blue(red) in (a) and (b).



297 FIG. 9. Evolution of zonal wind from 54S to 80S for the [ozone hole-PI] runs for an aquaplanet (a) with  
 298 “Antarctic” albedo equal to 0.27 (AQUA27), (b) with “Antarctic” albedo equal to 0.8 (AQUA80). (c) difference  
 299 between (a) and (b). The 1m/s contour is indicated in red in (a) and (b).

327 This negative feedback caused by the presence of stationary waves can be further demonstrated  
 328 by imposing the same ozone hole in the Northern Hemisphere. We compare the response of



300 FIG. 10. Evolution of subpolar U for the (a) [ozone hole-PI] runs with (blue) realistic stationary waves, (red)  
 301 an aquaplanet with “Antarctic” albedo equal to 0.27, (black) an aquaplanet with “Antarctic” albedo equal to 0.8,  
 302 and (gold) Northern Hemisphere with realistic stationary waves. (b) runs analogous to [ozone hole-PI] but in  
 303 which a diabatic heating perturbation is imposed directly (see methods). The mean of each fifteen day segment  
 304 after branching is indicated with a dot, and is labeled by the last day included in the fifteen day segment (e.g. 30  
 305 is for days 16 to 30). For (b), for the runs with a factor of five increase in diabatic heating rate, we divide the  
 306 response by a factor of five.

329 subpolar zonal wind in the (y-axis) lower stratosphere and (x-axis) lower troposphere in Figure 10.  
 330 Consider STAT (blue line); the average wind anomaly for days 61 to 75 is 8.8m/s at 70hPa and  
 331 1.0m/s at 850hPa, whereas in the two AQUA runs the wind responses are stronger (for AQUA80 in  
 332 black, 10.8m/s at 70hPa and 2.0m/s at 850hPa). The corresponding changes for the NH (in gold)  
 333 are much weaker both in the lower stratosphere and troposphere despite cooling aloft (4.0m/s and  
 334 0.3m/s respectively). The net effect is that stationary waves (of which there is more activity in the  
 335 NH) help damp the surface response to ozone depletion. The stationary wave effect will be further  
 336 isolated in Section 5c

337 It is important to note that while stationary waves damp the surface response, transient planetary  
 338 waves help contribute to the surface response, in agreement with Smith and Scott (2016). We  
 339 demonstrate this by considering the Eulerian mean momentum budget for AQUA80 which only  
 340 contains transient planetary waves. The zonal wind tendency calculated explicitly is shown in  
 341 Figure 11abc, and the various terms in terms of the budget (equation 2) are shown in the rest of  
 342 Figure 11. Figure 11def shows the sum of all terms on the right-hand side of equation 2, which

343 should be equal to the zonal wind tendency in Figure 11abc. This is indeed the case, as the budget  
344 closes in nearly all regions, though some of the fine-scale details of the wind tendencies differ. The  
345 dominant terms are the eddy forcing term (Figure 11ghi) and the coriolis torque (Figure 11jkl),  
346 with the acceleration in most regions and lags provided by the eddy forcing term. The sum of  
347 the eddy forcing and coriolis terms (Figure 11mno) already resembles the total tendency in most  
348 regions/lags (Figure 11def), but crucially in the mid- and upper- stratosphere changes in gravity  
349 wave absorption act as a negative feedback in days 31 to 70 (late spring), and dominate the response  
350 in days 71 to 120 (summer). In other words, the zonal wind anomaly peaks in December before  
351 weakening in January and February because the already accelerated vortex allows for more gravity  
352 wave absorption in the mid-stratosphere. The advection term also contributes in regions with  
353 strong wind gradients (bottom, Figure 11). The net effect is that the dominant term for the subpolar  
354 zonal acceleration is the resolved eddy term in Figure 11ghi, and importantly this acceleration  
355 extends from the stratosphere to the surface.

356 Figure 12 decomposes the eddy forcing into its various wavenumber components. At early lags,  
357 the tropospheric response arises mostly through wave-2 and wave-3 (Figure 12def), while for days  
358 71 to 120 synoptic wavenumbers are most important (Figure 12ghi). The wave-2 and wave-3  
359 present in AQUA80 are transient planetary waves, and it is clear that they help set up the initial jet  
360 shift and then contribute a continued acceleration at subpolar latitudes. Wave-1 does not contribute  
361 to forcing the jet shift (Figure 12abc). These conclusions are true of the STAT runs as well (Figure  
362 14).

363 The importance of both planetary and synoptic waves is also evident using the Transformed  
364 Eulerian mean budget (as in Orr et al. 2012b). The time evolution of the upper tropospheric  
365 (200-400hPa) meridional component of the Eliassen Palm flux ( $EP_y$ ) is shown in Figure 3de and  
366 6de for STAT and AQUA80; both synoptic and planetary waves are important. The timing of the  
367 increase in  $EP_y$  is similar for both synoptic and planetary waves, however, and thus it is unclear  
368 if one can be argued to help induce the other. That being said, these figures (and also Figure 12)  
369 show that at later lags, synoptic wavenumbers dominate the response. A similar relative role for  
370 planetary waves vs. synoptic waves for the tropospheric jet shift is evident for both AQUA80 and  
371 STAT (in both Figure 3de and 6de), and hence the presence of stationary waves does not appear to  
372 affect the ability of planetary waves to contribute to the jet shift. However the jet shift is weaker

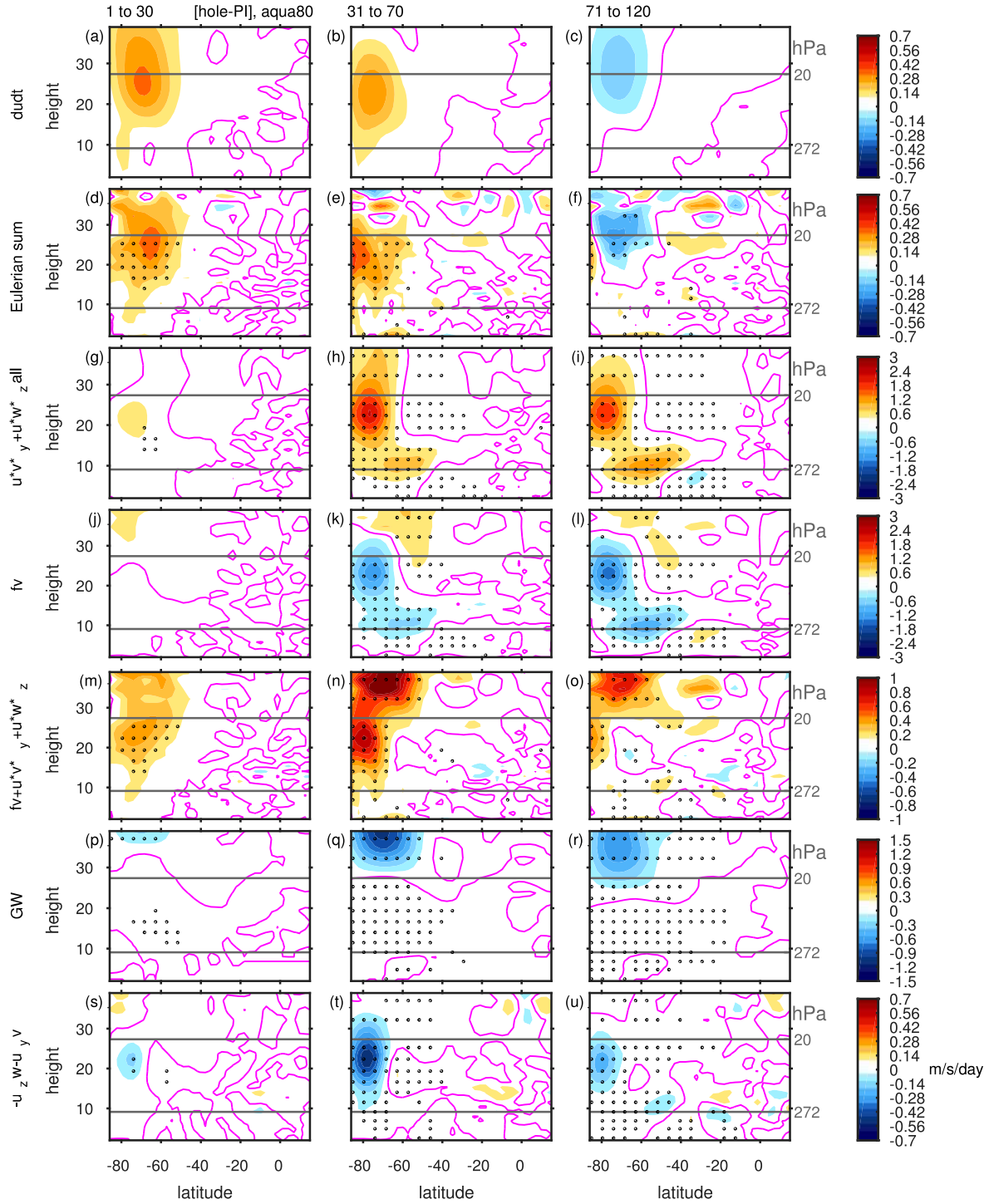
373 for STAT (due to surface shortwave and stationary wave feedbacks) and consistent with this the  
374 overall eddy forcing is weaker too (Figure 3de vs. 6de).

386 *c. Response of STAT and AQUA80 to stratospheric diabatic heating*

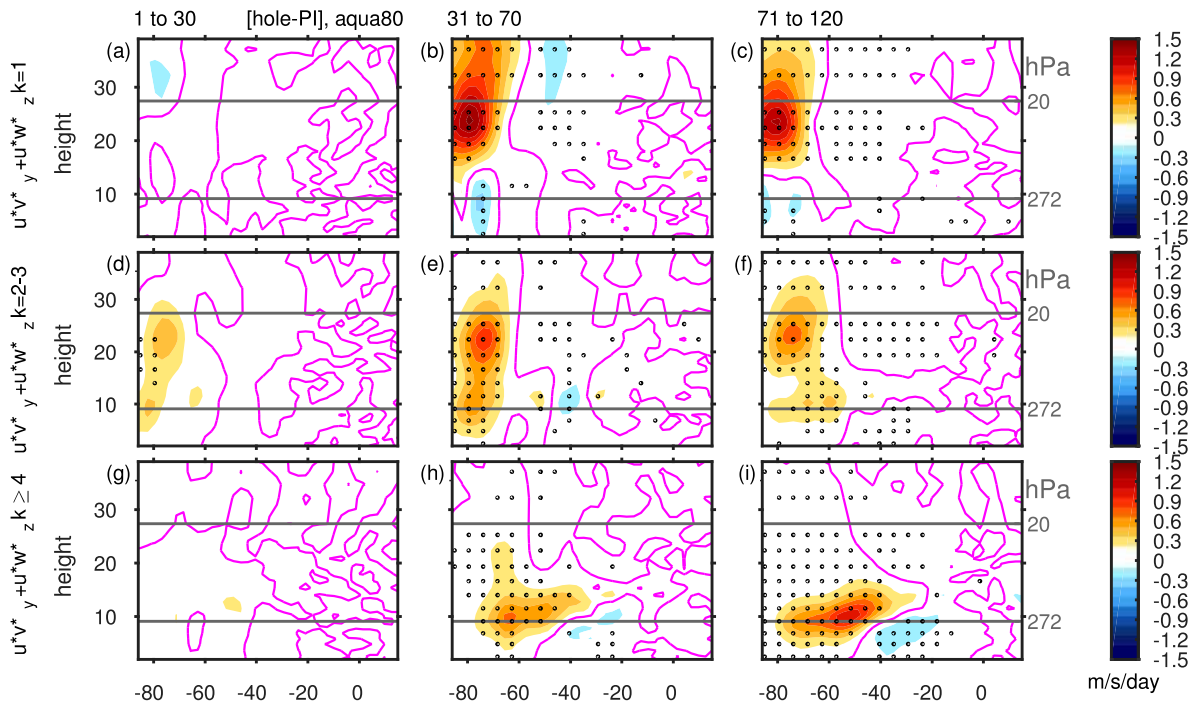
387 In addition to the ozone hole runs presented thus far, we have also performed integrations in  
388 which a diabatic heating perturbation replaces the ozone perturbation. As discussed in Section  
389 2, the spatial structure of the diabatic heating perturbation follows the ozone perturbation, and its  
390 magnitude (-0.5K/day) mimics that due to ozone (Figure 1d-f). The benefit from these diabatic  
391 heating runs are two-fold: first, we can increase the amplitude of this diabatic heating perturbation  
392 at will and hence explore linearity of the response. (In contrast, the impact of ozone saturates  
393 as concentrations cannot be negative.) Second, the surface shortwave heating perturbation is not  
394 present, and hence the stationary waves present in STAT but absent in AQUA80 are the only factor  
395 that can lead to a difference in the surface response.

396 We begin with the linearity of the response. Figure 10b is similar to Figure 10a, but showing the  
397 response to a diabatic heating perturbation imposed on STAT and AQUA80. By construction, the  
398 lower stratospheric and tropospheric wind response for a -0.5K/day perturbation (the dark purple  
399 and dark gray lines) in Figure 10b resemble qualitatively their counterpart in Figure 10a. The  
400 experiments with a factor of five times stronger perturbation (-2.5K/day) are shown in Figure 10b  
401 but with the subsequent response divided by a factor of five. It is clear that the response is generally  
402 linear. (The response in AQUA80 is slightly weaker than might be expected by linearity, though  
403 the response for STAT is stronger). This result highlights the fact that interannual variability in  
404 ozone concentrations should be useful for seasonal predictability of surface climate (Son et al.  
405 2013; Bandoro et al. 2014; Hendon et al. 2020; Jucker and Goyal 2021).

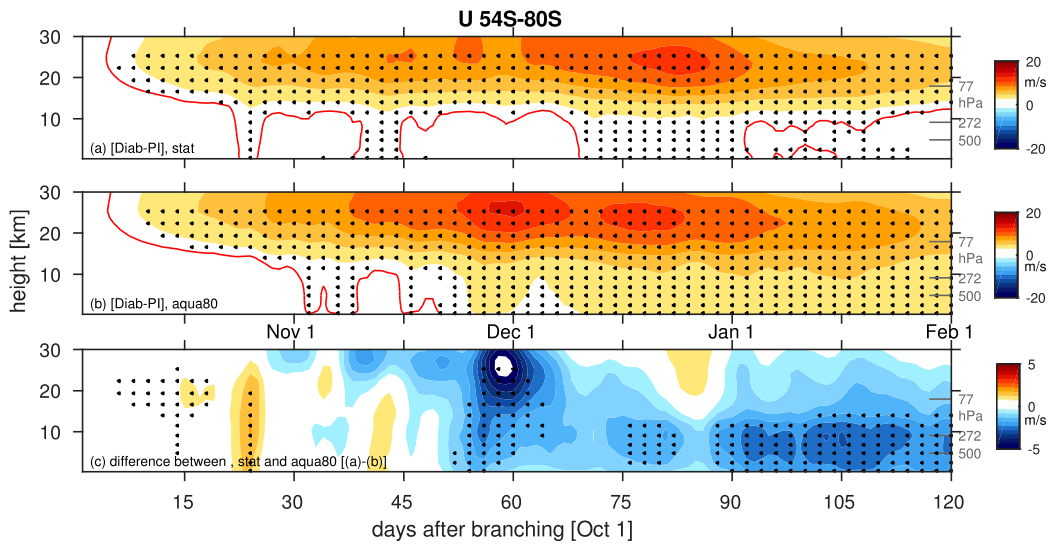
406 Next, we use these diabatic forcing experiments to isolate the role of stationary waves for  
407 the downward response, as these experiments do not allow for the shortwave surface feedback  
408 mechanism from Section 5a. The subpolar zonal wind response for STAT and AQUA80 to an  
409 identical perturbation is shown in Figure 13a and 13b, and the difference between the two is in  
410 Figure 13c. Initially, the diabatic perturbation causes a larger response in STAT, but the zonal wind  
411 response in AQUA80 in both the stratosphere and troposphere becomes larger after day 45. Hence,  
412 stationary waves lead to a negative feedback on the response even if surface shortwave feedbacks



375 FIG. 11. Eulerian mean momentum budget for the [ozone hole-PI] aquaplanet runs, with “Antarctic” albedo  
 376 equal to 0.8 in (left) days 1-30 after branching, i.e. October; (middle) days 31 to 70; (right) days 71 to 120. (a-c)  
 377 total wind tendency; (d-f) sum of all terms; (g-i) eddy forcing terms ( $u'v'$  and  $u'w'$ ); (j-l) coriolis torque; (m-o)  
 378 sum of eddy forcing and coriolis torque; (p-r) gravity wave drag; (s-u) advection of mean zonal wind. Note that  
 379 the color-bar for (g-i) and (j-l) differ from that in (m-o) due to the strong cancellation between eddy forcing and  
 380 coriolis torque (as expected).



381 FIG. 12. Decomposition of the eddy forcing term in 11ghi into the various wavenumber components. (a-c)  
 382 wavenumber 1; (d-f) wavenumber 2 through 3; (g-i) wavenumbers 4 and larger.



383 FIG. 13. Evolution of zonal wind from 54S to 80S for the Diabatic-PI runs with (a) realistic stationary waves,  
 384 (b) an aquaplanet, with “Antarctic” albedo equal to 0.8. (c) difference between (a) and (b). The 1m/s contour is  
 385 indicated in red in (a) and (b).

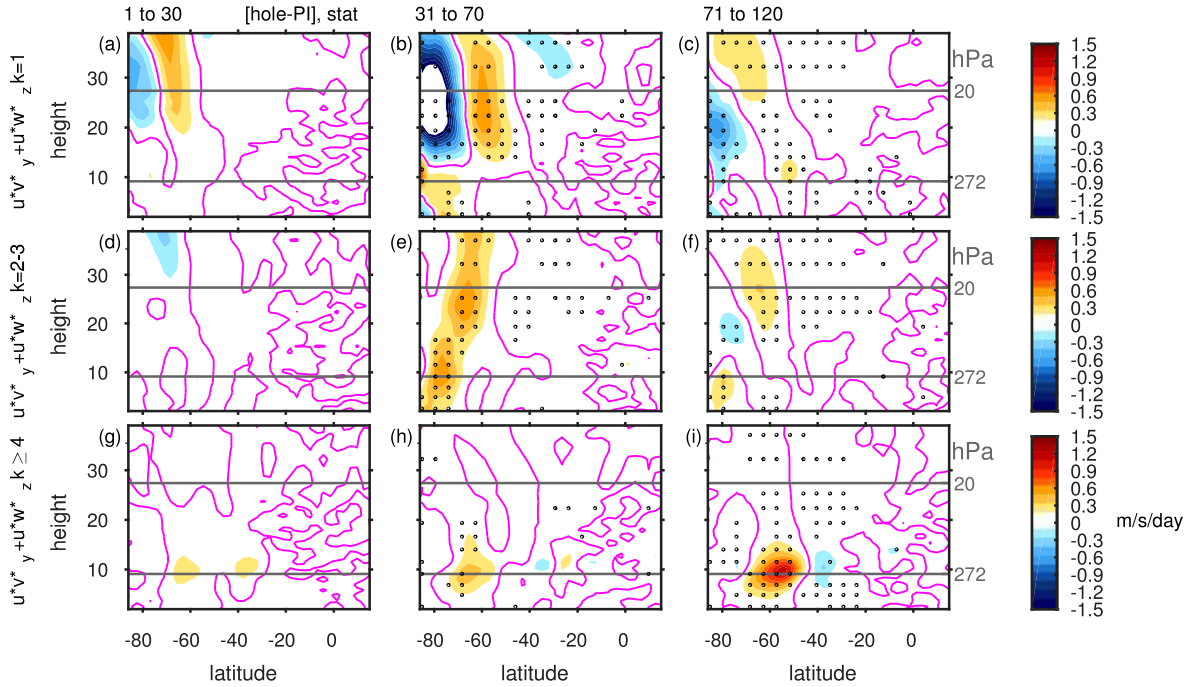


FIG. 14. As in 12 but for STAT.

413 are suppressed, but this stationary wave feedback develops slowly. We speculate that the stationary  
 414 wave effect is connected to the delayed breakup of the vortex; it manifests itself only late in the  
 415 season when the vortex is already gone in the PI control simulation.

416 *d. Relative roles of stationary waves and shortwave feedbacks*

417 We have demonstrated that there are two distinct effects that lead to a weaker response to ozone  
 418 depletion in STAT as compared to AQUA80: surface shortwave feedbacks and stationary waves  
 419 that partially compensate the cooling of the pole due to ozone loss. The two effects were isolated in  
 420 Figure 9 (for shortwave feedbacks) and Figure 13 (for stationary wave feedbacks). This delineation  
 421 of the two effects allows us to ask the question: Which of the two is more important?

422 A comparison of Figure 9c and Figure 13c indicates that the shortwave effect is quicker to begin,  
 423 and is already present by day 20. Its amplitude subsequently increases over time as the summer  
 424 solstice is approached. In contrast, the stationary wave effect does not manifest itself until late in  
 425 the season when the vortex is already strengthened, and thus the difference in Figure 13c is only  
 426 significant after day 50 (late November). After the effect begins however, it is stronger than the  
 427 shortwave effect and persists with roughly similar magnitude through the rest of summer. The net

428 effect is that the shortwave effect is most important in November, the stationary wave effect is most  
429 important in December, and both are of roughly equal importance in January.

## 430 **6. Discussion and Conclusions**

431 Ozone depletion is known to have been the dominant contributor to a poleward shift of the  
432 Southern Hemisphere (SH) tropospheric midlatitude jet, precipitation, and storm tracks over the  
433 late 20th century. Over the next 50 years, ozone recovery is expected to nearly cancel out changes  
434 in the jet and Hadley Cell that would otherwise be forced by greenhouse gases (Polvani et al. 2011;  
435 Arblaster et al. 2011; Barnes and Polvani 2013; Gerber and Son 2014; Waugh et al. 2015; Seviour  
436 et al. 2017; Son et al. 2018; Banerjee et al. 2020). The degree of cancellation is uncertain and  
437 model dependent, however, leading to uncertainty in future projections (Gerber and Son 2014).  
438 The mechanism whereby ozone depletion leads to a downward impact, and the details of how  
439 this mechanism governs the magnitude of the impact, are still unclear (as noted in WMO Ozone  
440 assessments in 2010, 2014, and 2018). While previous work has shown that jet latitude (Garfinkel  
441 et al. 2013b) and the details of the ozone forcing (Neely et al. 2014; Young et al. 2014) are  
442 important, we have demonstrated two additional processes that are important for the downward  
443 impact: surface shortwave effects and stationary waves.

444 This study takes advantage of a recently developed intermediate complexity model that can  
445 delineate the role of these two effects. First, we integrate it with realistic stationary waves,  
446 comparing it to runs without any zonal asymmetry in the bottom boundary. Second, we compared  
447 integrations with an ozone hole in which surface shortwave feedbacks are present, to integrations  
448 with a diabatic temperature tendency that mimics the shortwave effects of ozone depletion in the  
449 stratosphere only. This flexibility allowed us to isolate the role of stationary waves and surface  
450 shortwave changes for the surface response.

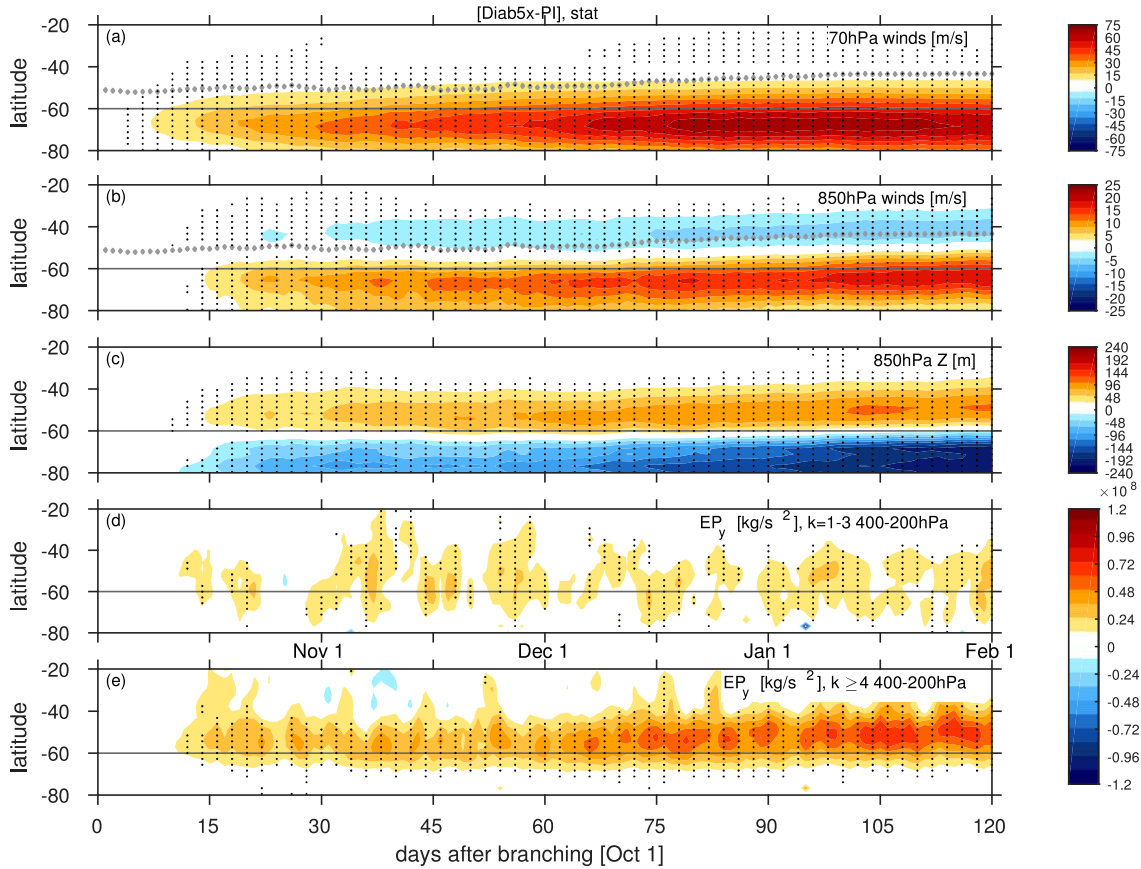
451 In the most realistic configuration (STAT), the model simulates a response resembling that  
452 observed and simulated by comprehensive models (Figure 1, 2, and 3). When an identical ozone  
453 hole is imposed in an aquaplanet configuration (AQUA80), the response is twice as strong for many  
454 of the diagnostics examined (Figure 1mno, 5, and 6). The realistic and aquaplanet configurations  
455 differ in at least two aspects potentially relevant to the ozone hole response: stationary waves and  
456 surface shortwave effects.

457 The importance of surface shortwave effects was isolated by comparing an aquaplanet config-  
458 uration with an albedo of 0.8 over Antarctica (AQUA80) to a similar configuration but with an  
459 albedo of 0.27 (AQUA27; Figure 9), as the stationary waves are identical in these configurations.  
460 The poleward jet shift is significantly stronger in AQUA80 than in AQUA27 by late October, and  
461 in January the tropospheric response is more than a factor of two stronger in AQUA80. The  
462 stratospheric response is also stronger in AQUA80 because the colder lower tropospheric column  
463 also impacts geopotential height in the stratosphere, as can be diagnosed using the hypsometric  
464 equation.

465 The importance of stationary waves was isolated by comparing the response to a stratospheric  
466 diabatic heating perturbation of similar strength and spatial structure to that caused by ozone  
467 depletion in both AQUA80 and STAT (Figure 13ab). The only factor that can explain a difference  
468 in response (Figure 13c) is a stationary wave feedback, as surface shortwave effects are not  
469 present. The presence of stationary waves leads to a weaker response starting in late November and  
470 extending into February to an identical diabatic heating perturbation. This effect arises because a  
471 stationary wave negative feedback leads to a weaker stratospheric circulation response when there  
472 are stationary waves in the troposphere.

473 Despite the negative stationary wave feedback on the magnitude of the stratospheric circulation  
474 response to ozone depletion, tropospheric planetary waves are important for the tropospheric jet  
475 response. Both planetary and synoptic waves are important for the tropospheric jet shift both in  
476 AQUA80 and STAT integrations (Figures 12 and 14). Waves 1-3 contribute roughly half of the  
477 torque in November, though by December and January their contribution is less (Figure 3de and  
478 6de). This is true for both of the ozone depletion runs, and also the diabatic heating runs where  
479 we can increase the amplitude of the forcing to better capture the response (Figure 15).

482 Gravity waves also act as a negative feedback on the magnitude of the stratospheric circulation  
483 response to ozone depletion. Namely, the strengthened polar vortex allows more gravity waves to  
484 propagate into the stratosphere, and these gravity waves then break in the subpolar mid-stratosphere  
485 (Figure 11). This partial compensation between gravity waves and an externally imposed forcing  
486 is consistent with Cohen et al. (2013); Sigmond and Shepherd (2014); Scheffler and Pulido (2015);  
487 Watson and Gray (2015), and Garfinkel and Oman (2018).



480 FIG. 15. As in Figure 3 but for a diabatic heating rate of 2.5K/day in the lower stratosphere and no ozone  
 481 depletion. Note factor of 5 difference in colorbar for (a) and (b), and factor of 2 difference for (c)-(e).

488 The response in AQUA27 is weaker than in AQUA80 despite the fact that the jet is further  
 489 equatorward and the annular mode timescale larger in AQUA27, two factors that would lead to  
 490 a stronger response (Garfinkel et al. 2013b). This indicates that the surface shortwave effect in  
 491 AQUA27 overwhelms the jet latitude/eddy feedback strength effect. In order to cleanly assess  
 492 the eddy feedback strength effect highlighted by Garfinkel et al. (2013b), we have performed an  
 493 experiment using the AQUA80 configuration but in which the jet is pushed 7° further poleward.  
 494 This is achieved by imposing a stronger and more poleward meridional ocean heat transport gradient  
 495 following equation A8 of Garfinkel et al. (2020a) with an amplitude of  $50Wm^{-2}$ , which leads to a  
 496 poleward shift of the sea surface temperature gradient. The response to ozone depletion is shown  
 497 in supplemental Figure 1, and it is clear that the tropospheric response is weaker as expected. The  
 498 stationary waves and surface shortwave effects are identical in this simulation to those in AQUA80,

499 and hence the weakened tropospheric response is due to jet latitude and weakened eddy feedback.  
500 Note that this run includes a stronger sea surface temperature front than AQUA80 yet has a weaker  
501 response, suggesting that the results of Ogawa et al. (2015) may have more to do with the eddy  
502 feedback strength in their simulations than the well-defined sea surface temperature front per se.

503 The specific mechanism as to how the downward influence arises is not the main focus of this  
504 paper, however our results are of relevance to previously proposed theories. Wave-2 and wave-3 are  
505 crucial in the lower stratospheric zonal momentum response ( Figures 12 and 14, consistent with  
506 Orr et al. 2012b). Both planetary and synoptic waves are important for the tropospheric impact, and  
507 it is impossible to distinguish whether one begins before the other. This difficulty occurs even if we  
508 enhance the signal-to-noise ratio by imposing a diabatic heating perturbation five times stronger  
509 than that associated with ozone depletion (Figure 15de), likely because of eddy-eddy interactions  
510 (Domeisen et al. 2013; Smith and Scott 2016). Synoptic waves are somewhat more important in  
511 summer, but in late fall the momentum forcing is more evenly split between synoptic and planetary  
512 waves. This balance is evident both in AQUA80 and in STAT.

513 In all runs, a tropospheric response does not begin until at least day 15, and in the diabatic heating  
514 runs with the forcing increased by a factor of five, there is even a weak equatorward shift in the first  
515 ten days (though not evident in Figure 15b using the chosen contour interval). This arises because  
516 a thermally driven cooling of the vortex will be balanced in part by downwelling over the pole  
517 and equatorward motion in the troposphere, which leads to an easterly Coriolis torque (Eliassen  
518 1951). This opposite response is consistent with Yang et al. (2015) who also find that the residual  
519 circulation is of the wrong sign to explain the poleward shift, and also with White et al. (2020)  
520 who also impose a diabatic heating perturbation and find that the poleward shift does not occur for  
521 at least 15 days. This effect does not explain why the observed poleward shift is not robust until  
522 December, however, as this delay is far longer than 15 days.

523 On the other hand, our simulations help clarify the important factors for the onset of the response.  
524 Namely, the tropospheric response can begin in late October if the forcing is strong (Figure 15b)  
525 or in AQUA80 (Figure 6b). The tropospheric response begins first at subpolar latitudes and only  
526 later, after synoptic eddies dominate, includes the midlatitudes. The net effect is that the delay  
527 until December in STAT is a consequence of the two negative feedbacks - stationary waves and  
528 surface shortwave effects - that both weaken and postpone the response until after the ozone hole

529 is already filling up. Future work should evaluate whether these negative feedbacks are crucial for  
530 the timing of the onset of the response in observations as well.

531 The response to an identical ozone hole imposed in the Northern Hemisphere in STAT (STATNH)  
532 is significantly weaker than when imposed in the Southern Hemisphere (Supplemental Figure 2).  
533 In other words, the tropospheric circulation in the Northern Hemisphere is less sensitive to a  
534 stratospheric ozone perturbation. Both of the negative feedbacks we identified - stationary waves  
535 and surface shortwave effects - likely play a role. Northern Hemisphere stationary waves are  
536 stronger, and hence the stratospheric circulation response to an identical ozone depletion is weaker  
537 due to an offset by enhanced wave propagation into the stratosphere. Second, the Arctic includes  
538 more regions with lower albedo as compared to the Antarctic. In addition, the annular mode  
539 timescale is shorter in the Northern Hemisphere (22 days; Figure 10), and hence synoptic eddy  
540 feedbacks are weaker too.

541 While the model used in this work suffers from some limitations - there is no coupling of  
542 the ozone with the dynamics, the imposed ozone hole has no zonal structure, and the albedo is  
543 constant for all shortwave wavelengths - the results of our work have implications for seasonal  
544 forecasting and for the interpretation of results from both comprehensive and idealized models.  
545 First, interannual variability in ozone concentrations can be used to enhance seasonal forecasting  
546 (Figure 10), consistent with Hendon et al. (2020) and Jucker and Goyal (2021). Second, dry and  
547 flat idealized models miss both the stationary wave and shortwave effects, and the lack of these  
548 effects can lead to an exaggerated doubling of the response to an identical ozone hole. Third,  
549 the surface radiative budget over the Antarctic surface and boundary layer is crucial for getting  
550 the correct temperature response to ozone depletion for the right reasons, and it is not clear how  
551 well models can capture the stable boundary layers common over Antarctica, the mixed-phase and  
552 ice clouds common at these latitudes, or the properties of a glaciated land surface. Future work  
553 should explore whether diversity in how models represent these processes can explain some of  
554 the diversity in future projections of climate change in the Southern Hemisphere (Gerber and Son  
555 2014), and thereby help narrow projections as ozone recovers.

556 *Acknowledgments.* CIG and IW acknowledge the support of a European Research Council starting  
557 grant under the European Union Horizon 2020 research and innovation programme (grant agree-  
558 ment number 677756). EPG acknowledges support from the US NSF through grant AGS 1852727.

559 MJ acknowledges support from the Australian Research Council (ARC) Centre of Excellence for  
560 Climate Extremes (CE170100023) and ARC grant FL 150100035. SWS was supported by the  
561 National Research Foundation of Korea (NRF) grant funded by the Korea government (Ministry  
562 of Science and ICT 2017R1E1A1A01074889).

563 *Data availability statement.* The updated version of MiMA used in  
564 this study including the modified source code can be downloaded from  
565 <https://github.com/ianpwhite/MiMA/releases/tag/MiMA-ThermalForcing-v1.0beta> (with DOI:  
566 <https://doi.org/10.5281/zenodo.4523199>).

## 567 **References**

568 Andrews, D. G., J. R. Holton, and C. B. Leovy, 1987: *Middle Atmosphere Dynamics*. Academic  
569 Press.

570 Arblaster, J. M., G. A. Meehl, and D. J. Karoly, 2011: Future climate change in the southern  
571 hemisphere: Competing effects of ozone and greenhouse gases. *Geophysical Research Letters*,  
572 **38 (2)**.

573 Baldwin, M. P., D. B. Stephenson, D. W. J. Thompson, T. J. Dunkerton, A. J. Charlton, and  
574 A. O'Neill, 2003: Stratospheric memory and skill of extended-range weather forecasts. *Science*,  
575 **301**, doi:10.1126/science.1087143.

576 Bandoro, J., S. Solomon, A. Donohoe, D. W. Thompson, and B. D. Santer, 2014: Influences of  
577 the antarctic ozone hole on southern hemispheric summer climate change. *Journal of Climate*,  
578 **27 (16)**, 6245–6264.

579 Banerjee, A., J. C. Fyfe, L. M. Polvani, D. Waugh, and K.-L. Chang, 2020: A pause in southern  
580 hemisphere circulation trends due to the montreal protocol. *Nature*, **579 (7800)**, 544–548.

581 Barnes, E. A., and L. Polvani, 2013: Response of the midlatitude jets, and of their variability,  
582 to increased greenhouse gases in the cmip5 models. *Journal of Climate*, **26 (18)**, 7117–7135,  
583 doi:10.1175/JCLI-D-12-00536.1.

584 Betts, A., and M. Miller, 1986: A new convective adjustment scheme. part ii: Single column  
585 tests using gate wave, bomex, atex and arctic air-mass data sets. *Quarterly Journal of the Royal*  
586 *Meteorological Society*, **112 (473)**, 693–709, doi:10.1002/qj.49711247308.

587 Betts, A. K., 1986: A new convective adjustment scheme. part i: Observational and theoretical  
588 basis. *Quarterly Journal of the Royal Meteorological Society*, **112 (473)**, 677–691, doi:10.1002/  
589 qj.49711247307.

590 Checa-Garcia, R., 2018: C mip6 ozone forcing dataset: supporting information. *Zenodo*, URL  
591 <https://doi.org/10.5281/zenodo.1135127>.

592 Checa-Garcia, R., M. I. Hegglin, D. Kinnison, D. A. Plummer, and K. P. Shine, 2018: Historical  
593 tropospheric and stratospheric ozone radiative forcing using the cmip6 database. *Geophysical*  
594 *Research Letters*, **45 (7)**, 3264–3273.

595 Chiodo, G., L. Polvani, and M. Previdi, 2017: Large increase in incident shortwave radiation due to  
596 the ozone hole offset by high climatological albedo over antarctica. *Journal of Climate*, **30 (13)**,  
597 4883–4890.

598 Cohen, N. Y., E. P. Gerber, and E. P. Oliver Bühler, 2013: Compensation between resolved and  
599 unresolved wave driving in the stratosphere: Implications for downward control. *Journal of the*  
600 *Atmospheric Sciences*, **70 (12)**, 3780–3798, doi:10.1175/JAS-D-12-0346.1.

601 Domeisen, D. I., L. Sun, and G. Chen, 2013: The role of synoptic eddies in the tropospheric  
602 response to stratospheric variability. *Geophysical research letters*, **40 (18)**, 4933–4937.

603 Eliassen, A., 1951: Slow thermally or frictionally controlled meridional circulation in a circular  
604 vortex. *Astrophysica Norvegica*, **5**, 19.

605 Eyring, V., and Coauthors, 2013: Long-term ozone changes and associated climate impacts in  
606 cmip5 simulations. *Journal of Geophysical Research: Atmospheres*, **118 (10)**, 5029–5060,  
607 doi:10.1002/jgrd.50316.

608 Frierson, D. M., I. M. Held, and P. Zurita-Gotor, 2006: A gray-radiation aquaplanet moist gcm.  
609 part i: Static stability and eddy scale. *Journal of the atmospheric sciences*, **63 (10)**, 2548–2566,  
610 doi:10.1175/JAS3753.1.

- 611 Frierson, D. M., I. M. Held, and P. Zurita-Gotor, 2007: A gray-radiation aquaplanet moist gcm.  
612 part ii: Energy transports in altered climates. *Journal of the atmospheric sciences*, **64** (5),  
613 1680–1693, doi:10.1175/JAS3913.1.
- 614 Garcia, R. R., D. E. Kinnison, and D. R. Marsh, 2012: “world avoided” simulations with the  
615 whole atmosphere community climate model. *Journal of Geophysical Research: Atmospheres*,  
616 **117** (D23).
- 617 Gardner, A. S., and M. J. Sharp, 2010: A review of snow and ice albedo and the development of  
618 a new physically based broadband albedo parameterization. *Journal of Geophysical Research:*  
619 *Earth Surface*, **115** (F1).
- 620 Garfinkel, C., and L. Oman, 2018: Effect of gravity waves from small islands in the southern  
621 ocean on the southern hemisphere atmospheric circulation. *Journal of Geophysical Research:*  
622 *Atmospheres*, **123** (3), 1552–1561.
- 623 Garfinkel, C., D. W. Waugh, and E. Gerber, 2013a: Effect of tropospheric jet latitude on coupling  
624 between the stratospheric polar vortex and the troposphere. *J. Clim.*, **26** (6), 2077–2095, doi:  
625 10.1175/JCLI-D-12-00301.1.
- 626 Garfinkel, C. I., D. W. Waugh, and E. P. Gerber, 2013b: The effect of tropospheric jet latitude on  
627 coupling between the stratospheric polar vortex and the troposphere. *Journal of Climate*, **26** (6),  
628 doi:10.1175/JCLI-D-12-00301.1.
- 629 Garfinkel, C. I., I. White, E. P. Gerber, and M. Jucker, 2020a: The impact of sst biases in the  
630 tropical east pacific and agulhas current region on atmospheric stationary waves in the southern  
631 hemisphere. *Journal of Climate*, **33** (21), 9351–9374.
- 632 Garfinkel, C. I., I. P. White, E. P. Gerber, and M. Jucker, 2020b: The building blocks  
633 of northern hemisphere wintertime stationary waves. *Journal of Climate*, **33** (13), doi:  
634 10.1175/JCLI-D-19-0181.1.
- 635 Gerber, E. P., and L. M. Polvani, 2009: Stratosphere-troposphere coupling in a relatively  
636 simple agcm: The importance of stratospheric variability. *J. Clim.*, **22**, 1920–1933, doi:  
637 10.1175/2008JCLI2548.1.

- 638 Gerber, E. P., L. M. Polvani, and D. Ancukiewicz, 2008: Annular mode time scales in the  
639 Intergovernmental Panel on Climate Change Fourth Assessment Report models. *Geophys. Res.  
640 Lett.*, **35**, L22707, doi:10.1029/2008GL035712.
- 641 Gerber, E. P., and S.-W. Son, 2014: Quantifying the summertime response of the austral jet  
642 stream and hadley cell to stratospheric ozone and greenhouse gases. *Journal of Climate*, **27**,  
643 doi:10.1175/JCLI-D-13-00539.1.
- 644 Gillett, N. P., and D. W. Thompson, 2003: Simulation of recent southern hemisphere climate  
645 change. *Science*, **302 (5643)**, 273–275.
- 646 Gonzalez, P. L., L. M. Polvani, R. Seager, and G. J. Correa, 2014: Stratospheric ozone depletion:  
647 a key driver of recent precipitation trends in south eastern south america. *Climate Dynamics*,  
648 **42 (7-8)**, 1775–1792.
- 649 Grenfell, T. C., S. G. Warren, and P. C. Mullen, 1994: Reflection of solar radiation by the antarctic  
650 snow surface at ultraviolet, visible, and near-infrared wavelengths. *Journal of Geophysical  
651 Research: Atmospheres*, **99 (D9)**, 18 669–18 684.
- 652 Grise, K. M., D. W. Thompson, and P. M. Forster, 2009: On the role of radiative processes in  
653 stratosphere–troposphere coupling. *Journal of climate*, **22 (15)**, 4154–4161.
- 654 Hendon, H., E.-P. Lim, and S. Abhik, 2020: Impact of interannual ozone variations on the down-  
655 ward coupling of the 2002 southern hemisphere stratospheric warming. *Journal of Geophysical  
656 Research: Atmospheres*, **125 (16)**, e2020JD032 952.
- 657 Hendon, H. H., D. W. Thompson, and M. C. Wheeler, 2007: Australian rainfall and surface tem-  
658 perature variations associated with the southern hemisphere annular mode. *Journal of Climate*,  
659 **20 (11)**, 2452–2467.
- 660 Hitchcock, P., and I. R. Simpson, 2016: Quantifying eddy feedbacks and forcings in the tropospheric  
661 response to stratospheric sudden warmings. *Journal of the Atmospheric Sciences*, **73 (9)**, 3641–  
662 3657.
- 663 Hurwitz, M. M., P. A. Newman, and C. I. Garfinkel, 2011: The Arctic vortex in March 2011: a  
664 dynamical perspective. *Atm. Chem. Phys.*, **11**, 11 447–11 453, doi:10.5194/acp-11-11447-2011.

665 Hurwitz, M. M., P. A. Newman, F. Li, L. D. Oman, O. Morgenstern, P. Braesicke, and J. A.  
666 Pyle, 2010: Assessment of the breakup of the Antarctic polar vortex in two new chemistry-  
667 climate models. *Journal of Geophysical Research (Atmospheres)*, **115**, D07 105, doi:10.1029/  
668 2009JD012788.

669 Iacono, M. J., E. J. Mlawer, S. A. Clough, and J.-J. Morcrette, 2000: Impact of an improved  
670 longwave radiation model, rrtm, on the energy budget and thermodynamic properties of the near  
671 community climate model, ccm3. *Journal of Geophysical Research: Atmospheres*, **105 (D11)**,  
672 14 873–14 890.

673 Jucker, M., and E. Gerber, 2017: Untangling the annual cycle of the tropical tropopause layer with  
674 an idealized moist model. *Journal of Climate*, **30 (18)**, 7339–7358.

675 Jucker, M., and R. Goyal, 2021: Ozone-forced southern annular mode during antarctic stratospheric  
676 warming events. *Earth and Space Science Open Archive ESSOAr*.

677 Kållberg, P., P. Berrisford, B. Hoskins, A. Simmons, S. Lamy-thépaut, and R. Hine, 2005: *ERA-40*  
678 *atlas*. ERA-40 Project Report Series 19, ECMWF, 103 pp.

679 Kang, S. M., L. M. Polvani, J. C. Fyfe, and M. Sigmond, 2011: Impact of Polar Ozone Depletion  
680 on Subtropical Precipitation. *Science*, **332**, 951–, doi:10.1126/science.1202131.

681 Karpechko, A. Y., A. L. A. Maycock, M. Abalos, H. Akiyoshi, J. Arblaster, C. Garfinkel,  
682 K. Rosenlof, and M. Sigmond, 2018: *Stratospheric Ozone Changes and Climate, Chapter*  
683 *5 in Scientific Assessment of Ozone Depletion*. Global Ozone Research and Monitoring Project  
684 Rep. No. 58, 416 pp.

685 Kidson, J. W., 1988: Interannual variations in the southern hemisphere circulation. *Journal of*  
686 *Climate*, **1 (12)**, 1177–1198.

687 Kushner, P. J., and L. M. Polvani, 2004: Stratosphere-troposphere coupling in a relatively simple  
688 agcm: The role of eddies. *J. Clim.*, **17**, 629–639.

689 Lawrence, Z. D., J. Perlwitz, A. H. Butler, G. L. Manney, P. A. Newman, S. H. Lee, and E. R. Nash,  
690 2020: The remarkably strong arctic stratospheric polar vortex of winter 2020: Links to record-  
691 breaking arctic oscillation and ozone loss. *Journal of Geophysical Research: Atmospheres*,  
692 **125 (22)**, e2020JD033 271.

- 693 Li, F., P. A. Newman, and R. S. Stolarski, 2010: Relationships between the brewer-dobson  
694 circulation and the southern annular mode during austral summer in coupled chemistry-climate  
695 model simulations. *Journal of Geophysical Research: Atmospheres*, **115** (D15).
- 696 Manney, G. L., and Coauthors, 2011: Unprecedented arctic ozone loss in 2011. *Nature*, **478** (7370),  
697 469–475.
- 698 Manzini, E., B. Steil, C. Brühl, M. A. Giorgetta, and K. Krüger, 2003: A new interactive chemistry-  
699 climate model: 2. sensitivity of the middle atmosphere to ozone depletion and increase in  
700 greenhouse gases and implications for recent stratospheric cooling. *Journal of Geophysical*  
701 *Research: Atmospheres*, **108** (D14).
- 702 McLandress, C., A. I. Jonsson, D. A. Plummer, M. C. Reader, J. F. Scinocca, and T. G. Shepherd,  
703 2010: Separating the dynamical effects of climate change and ozone depletion. part i: Southern  
704 hemisphere stratosphere. *Journal of Climate*, **23** (18), 5002–5020, doi:10.1175/2010JCLI3586.  
705 1.
- 706 McLandress, C., T. G. Shepherd, J. F. Scinocca, D. A. Plummer, M. Sigmond, A. I. Jonsson, and  
707 M. C. Reader, 2011: Separating the dynamical effects of climate change and ozone depletion.  
708 part ii: Southern hemisphere troposphere. *Journal of Climate*, **24** (6), 1850–1868.
- 709 Merlis, T. M., T. Schneider, S. Bordoni, and I. Eisenman, 2013: Hadley circulation response to  
710 orbital precession. part ii: Subtropical continent. *Journal of Climate*, **26** (3), 754–771.
- 711 Mlawer, E. J., S. J. Taubman, P. D. Brown, M. J. Iacono, and S. A. Clough, 1997: Radiative transfer  
712 for inhomogeneous atmospheres: Rrtm, a validated correlated-k model for the longwave. *Journal*  
713 *of Geophysical Research: Atmospheres*, **102** (D14), 16 663–16 682.
- 714 Neely, R., D. Marsh, K. Smith, S. Davis, and L. Polvani, 2014: Biases in southern hemisphere  
715 climate trends induced by coarsely specifying the temporal resolution of stratospheric ozone.  
716 *Geophysical Research Letters*, **41** (23), 8602–8610, doi:10.1002/2014GL061627.
- 717 Newman, P., and Coauthors, 2009: What would have happened to the ozone layer if chlorofluoro-  
718 carbons (cfc) had not been regulated? *Atmospheric Chemistry and Physics*, **9** (6), 2113–2128.

- 719 Ogawa, F., N.-E. Omrani, K. Nishii, H. Nakamura, and N. Keenlyside, 2015: Ozone-induced  
720 climate change propped up by the southern hemisphere oceanic front. *Geophysical Research*  
721 *Letters*, **42** (22), 10–056.
- 722 Orr, A., T. J. Bracegirdle, J. S. Hosking, W. Feng, H. K. Roscoe, and J. D. Haigh, 2012a: Strong  
723 dynamical modulation of the cooling of the polar stratosphere associated with the antarctic ozone  
724 hole. *Journal of Climate*, **26** (2), 662–668.
- 725 Orr, A., T. J. Bracegirdle, J. S. Hosking, T. Jung, J. D. Haigh, T. Phillips, and W. Feng, 2012b:  
726 Possible dynamical mechanisms for southern hemisphere climate change due to the ozone hole.  
727 *Journal of the Atmospheric Sciences*, **69** (10), 2917–2932.
- 728 Polvani, L. M., M. Previdi, and C. Deser, 2011: Large cancellation, due to ozone recovery,  
729 of future southern hemisphere atmospheric circulation trends. *Geophysical Research Letters*,  
730 **38** (4), doi:DOI:10.1029/2011GL046712.
- 731 Polvani, L. M., D. W. Waugh, G. J. P. Correa, and S.-W. Son, 2011: Stratospheric Ozone Deple-  
732 tion: The Main Driver of Twentieth-Century Atmospheric Circulation Changes in the Southern  
733 Hemisphere. *Journal of Climate*, **24**, 795–812, doi:10.1175/2010JCLI3772.1.
- 734 Previdi, M., and L. M. Polvani, 2014: Climate system response to stratospheric ozone depletion and  
735 recovery. *Quarterly Journal of the Royal Meteorological Society*, **140** (685), 2401–2419, doi:  
736 <https://doi.org/10.1002/qj.2330>, URL [https://rmets.onlinelibrary.wiley.com/doi/abs/10.1002/qj.](https://rmets.onlinelibrary.wiley.com/doi/abs/10.1002/qj.2330)  
737 [2330](https://rmets.onlinelibrary.wiley.com/doi/pdf/10.1002/qj.2330), <https://rmets.onlinelibrary.wiley.com/doi/pdf/10.1002/qj.2330>.
- 738 Randel, W. J., and Coauthors, 2009: An update of observed stratospheric temperature trends.  
739 *Journal of Geophysical Research: Atmospheres*, **114** (D2), doi:10.1029/2008JD010421, URL  
740 <http://dx.doi.org/10.1029/2008JD010421>.
- 741 Rao, J., and C. I. Garfinkel, 2020: Arctic ozone loss in march 2020 and its seasonal prediction in  
742 cfsv2: A comparative study with the 1997 and 2011 cases. *Journal of Geophysical Research:*  
743 *Atmospheres*, **125** (21), e2020JD033 524.
- 744 Rao, J., and C. I. Garfinkel, 2021: The strong stratospheric polar vortex in march 2020 in sub-  
745 seasonal to seasonal models: Implications for empirical prediction of the low arctic total ozone  
746 extreme. *Journal of Geophysical Research: Atmospheres*, **126** (9), e2020JD034 190.

- 747 Scheffler, G., and M. Pulido, 2015: Compensation between resolved and unresolved wave drag  
748 in the stratospheric final warmings of the southern hemisphere. *Journal of the Atmospheric*  
749 *Sciences*, **72 (11)**, 4393–4411, doi:10.1175/JAS-D-14-0270.1.
- 750 Seviour, W. J., D. W. Waugh, L. M. Polvani, G. J. Correa, and C. I. Garfinkel, 2017: Robustness of  
751 the simulated tropospheric response to ozone depletion. *Journal of Climate*, **30 (7)**, 2577–2585.
- 752 Sheshadri, A., and R. A. Plumb, 2016: Sensitivity of the surface responses of an idealized agcm to  
753 the timing of imposed ozone depletion-like polar stratospheric cooling. *Geophysical Research*  
754 *Letters*, **43 (5)**, 2330–2336, doi:https://doi.org/10.1002/2016GL067964, URL https://agupubs.  
755 onlinelibrary.wiley.com/doi/abs/10.1002/2016GL067964, https://agupubs.onlinelibrary.wiley.  
756 com/doi/pdf/10.1002/2016GL067964.
- 757 Sigmund, M., and T. G. Shepherd, 2014: Compensation between resolved wave driving and  
758 parameterized orographic gravity wave driving of the brewer–dobson circulation and its response  
759 to climate change. *Journal of Climate*, **27 (14)**, 5601–5610, doi:10.1175/JCLI-D-13-00644.1.
- 760 Smith, K. L., and R. K. Scott, 2016: The role of planetary waves in the tropospheric jet response  
761 to stratospheric cooling. *Geophysical Research Letters*, **43 (6)**, 2904–2911, doi:https://doi.  
762 org/10.1002/2016GL067849, URL https://agupubs.onlinelibrary.wiley.com/doi/abs/10.1002/  
763 2016GL067849, https://agupubs.onlinelibrary.wiley.com/doi/pdf/10.1002/2016GL067849.
- 764 Solomon, S., R. R. Garcia, F. S. Rowland, and D. J. Wuebbles, 1986: On the depletion of Antarctic  
765 ozone. *nature*, **321**, 755–758, doi:10.1038/321755a0.
- 766 Solomon, S., R. W. Portmann, T. Sasaki, D. J. Hofmann, and D. W. Thompson, 2005: Four decades  
767 of ozonesonde measurements over antarctica. *Journal of Geophysical Research: Atmospheres*,  
768 **110 (D21)**.
- 769 Son, S.-W., E. P. Gerber, J. Perlwitz, L. M. Polvani, and C.-. collaborators, 2010: Impact of  
770 stratospheric ozone on Southern Hemisphere circulation change: A multimodel assessment.  
771 *Journal of Geophysical Research (Atmospheres)*, **115**, D00M07, doi:10.1029/2010JD014271.
- 772 Son, S.-W., A. Purich, H. H. Hendon, B.-M. Kim, and L. M. Polvani, 2013: Improved seasonal  
773 forecast using ozone hole variability? *Geophysical Research Letters*, **40 (23)**, 6231–6235.

- 774 Son, S.-W., and Coauthors, 2008: The impact of stratospheric ozone recovery on the southern  
775 hemisphere westerly jet. *Science*, **320 (5882)**, 1486–1489.
- 776 Son, S.-W., and Coauthors, 2018: Tropospheric jet response to antarctic ozone depletion: An  
777 update with chemistry-climate model initiative (ccmi) models. *Environmental Research Letters*,  
778 **13 (5)**, 054 024.
- 779 Stolarski, R. S., A. R. Douglass, M. Gupta, P. A. Newman, S. Pawson, M. R. Schoeberl, and J. E.  
780 Nielsen, 2006: An ozone increase in the Antarctic summer stratosphere: A dynamical response  
781 to the ozone hole. *Geophys. Res. Lett.*, **33**, L21805, doi:10.1029/2006GL026820.
- 782 Sun, L., G. Chen, and W. A. Robinson, 2014: The role of stratospheric polar vortex breakdown in  
783 southern hemisphere climate trends. *Journal of the Atmospheric Sciences*, **71 (7)**, 2335–2353.
- 784 Thompson, D. W., and J. M. Wallace, 2000: Annular modes in the extratropical circulation. part i:  
785 Month-to-month variability. *Journal of climate*, **13 (5)**, 1000–1016.
- 786 Thompson, D. W. J., S. Solomon, P. J. Kushner, M. H. England, K. M. Grise, and D. J. Karoly,  
787 2011: Signatures of the Antarctic ozone hole in Southern Hemisphere surface climate change.  
788 *Nature Geoscience*, **4**, 741–749, doi:10.1038/ngeo1296.
- 789 Trenberth, K. E., and D. P. Stepaniak, 2002: A pathological problem with NCEP reanalysis in the  
790 stratosphere. *J. Clim.*
- 791 Ummenhofer, C. C., A. S. Gupta, and M. H. England, 2009: Causes of late twentieth-century  
792 trends in new zealand precipitation. *Journal of Climate*, **22 (1)**, 3–19.
- 793 Watson, P. A., and L. J. Gray, 2015: The stratospheric wintertime response to applied extratropical  
794 torques and its relationship with the annular mode. *Climate Dynamics*, **44 (9-10)**, 2513–2537,  
795 doi:10.1007/s00382-014-2359-2.
- 796 Waugh, D. W., C. Garfinkel, and L. M. Polvani, 2015: Drivers of the recent tropical expansion  
797 in the southern hemisphere: Changing ssts or ozone depletion? *J. Clim.*, **28**, 6581–6586,  
798 doi:10.1175/JCLI-D-15-0138.1.
- 799 Weber, M., M. Coldewey-Egbers, V. E. Fioletov, S. M. Frith, J. D. Wild, J. P. Burrows, C. S.  
800 Long, and D. Loyola, 2018: Total ozone trends from 1979 to 2016 derived from five merged

801 observational datasets—the emergence into ozone recovery. *Atmospheric Chemistry and Physics*,  
802 **18 (3)**, 2097–2117.

803 White, I. P., C. I. Garfinkel, E. P. Gerber, M. Jucker, P. Hitchcock, and J. Rao, 2020: The generic  
804 nature of the tropospheric response to sudden stratospheric warmings. *Journal of Climate*,  
805 **33 (13)**, 5589–5610, doi:10.1175/JCLI-D-19-0697.1.

806 Wiscombe, W. J., and S. G. Warren, 1980: A model for the spectral albedo of snow. i: Pure snow.  
807 *Journal of the Atmospheric Sciences*, **37 (12)**, 2712–2733.

808 World Meteorological Organization, 2011: *Scientific Assessment of Ozone Depletion: 2010*. Global  
809 Ozone Research and Monitoring Project Rep. No. 52, 516 pp.

810 World Meteorological Organization, 2014: *Scientific Assessment of Ozone Depletion: 2014*. Global  
811 Ozone Research and Monitoring Project Rep. No. 55, 416 pp.

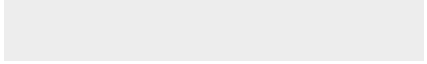
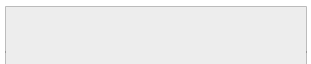
812 Yang, H., L. Sun, and G. Chen, 2015: Separating the mechanisms of transient responses to strato-  
813 spheric ozone depletion–like cooling in an idealized atmospheric model. *Journal of Atmospheric*  
814 *Sciences*, **72 (2)**, 763–773.

815 Yang, J., Q. Bao, D. Ji, D. Gong, R. Mao, Z. Zhang, and S.-J. Kim, 2014: Simulation and causes of  
816 eastern antarctica surface cooling related to ozone depletion during austral summer in fgoals-s2.  
817 *Advances in Atmospheric Sciences*, **31 (5)**, 1147–1156.

818 Young, P., S. Davis, B. Hassler, S. Solomon, and K. Rosenlof, 2014: Modeling the climate impact  
819 of southern hemisphere ozone depletion: The importance of the ozone data set. *Geophysical*  
820 *Research Letters*, **41 (24)**, 9033–9039, doi:10.1002/2014GL061738.



Click here to access/download  
**Supplemental Material**  
SHozonev7supplemental.pdf



1 **Supplement to: Stationary wave and surface radiative effects weaken and**  
2 **delay the near-surface response to stratospheric ozone depletion**

3 Chaim I. Garfinkel\*

4 *The Hebrew University of Jerusalem, Institute of Earth Sciences, Edmond J. Safra Campus, Givat*  
5 *Ram, Jerusalem, Israel*

6 Ian White

7 *The Hebrew University of Jerusalem, Institute of Earth Sciences, Edmond J. Safra Campus, Givat*  
8 *Ram, Jerusalem, Israel*

9 Edwin P. Gerber

10 *Courant Institute of Mathematical Sciences, New York University, New York, USA*

11 Seok-Woo Son

12 *School of Earth and Environmental Sciences, Seoul National University, Seoul, South Korea*

13 Martin Jucker

14 *Climate Change Research Centre and ARC Centre of Excellence for Climate Extremes,*  
15 *University of New South Wales, Sydney, Australia*

16 \*Corresponding author address: Chaim I. Garfinkel, The Hebrew University of Jerusalem, Institute  
17 of Earth Sciences, Edmond J. Safra Campus, Givat Ram, Jerusalem, Israel.

<sup>18</sup> E-mail: [chaim.garfinkel@mail.huji.ac.il](mailto:chaim.garfinkel@mail.huji.ac.il)

## ABSTRACT

<sup>19</sup> The main body documents some aspects of the response when an ozone hole  
<sup>20</sup> is placed in the Northern Hemisphere, and the supplement shows more. The  
<sup>21</sup> supplement also shows the response when the jet latitude is pushed poleward  
<sup>22</sup> for the AQUA80 configuration.

23 *Acknowledgments.* CIG, IW, and ME acknowledge the support of a European Research Coun-  
24 cil starting grant under the European Union Horizon 2020 research and innovation programme  
25 (grant agreement number 677756). EPG acknowledges support from the US NSF through grant  
26 AGS 1852727. MJ acknowledges support from the Australian Research Council (ARC) Centre  
27 of Excellence for Climate Extremes (CE170100023) and ARC grant FL 150100035. SWS was  
28 supported by the National Research Foundation of Korea (NRF) grant funded by the Korea gov-  
29 ernment (Ministry of Science and ICT 2017R1E1A1A01074889).

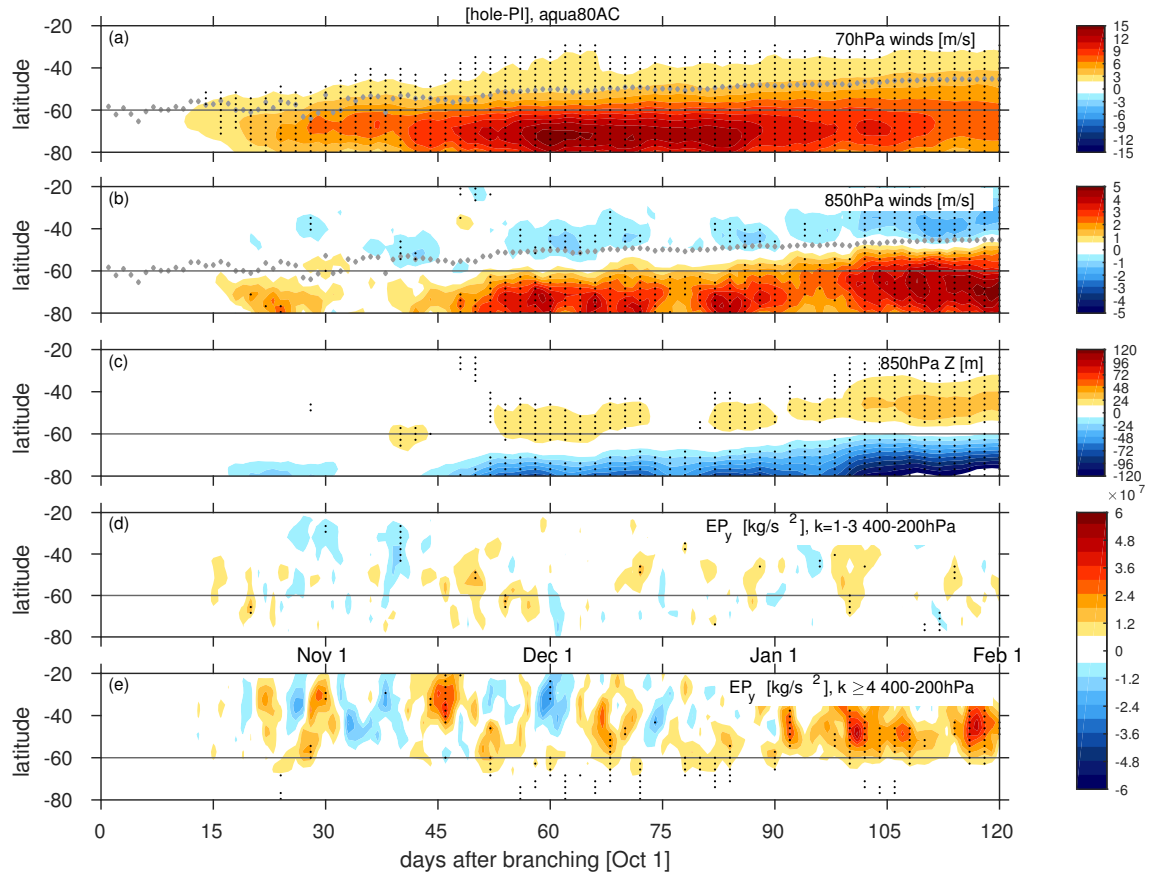
### 30 **References**

31 Garfinkel, C. I., I. White, E. P. Gerber, and M. Jucker, 2020: The impact of sst biases in the  
32 tropical east pacific and agulhas current region on atmospheric stationary waves in the southern  
33 hemisphere. *Journal of Climate*, **33** (21), 9351–9374.

34 **LIST OF FIGURES**

35 **Fig. 1.** As in Figure 6 of the main text but for a jet latitude  $7^\circ$  further poleward achieved by im-  
36 posing a north-south gradient in midlatitude ocean heat transport following equation A8 of  
37 Garfinkel et al. (2020). . . . . 6

38 **Fig. 2.** Zonal-mean responses for NH ozone hole. . . . . 7



39 FIG. 1. As in Figure 6 of the main text but for a jet latitude  $7^\circ$  further poleward achieved by imposing a  
 40 north-south gradient in midlatitude ocean heat transport following equation A8 of Garfinkel et al. (2020).

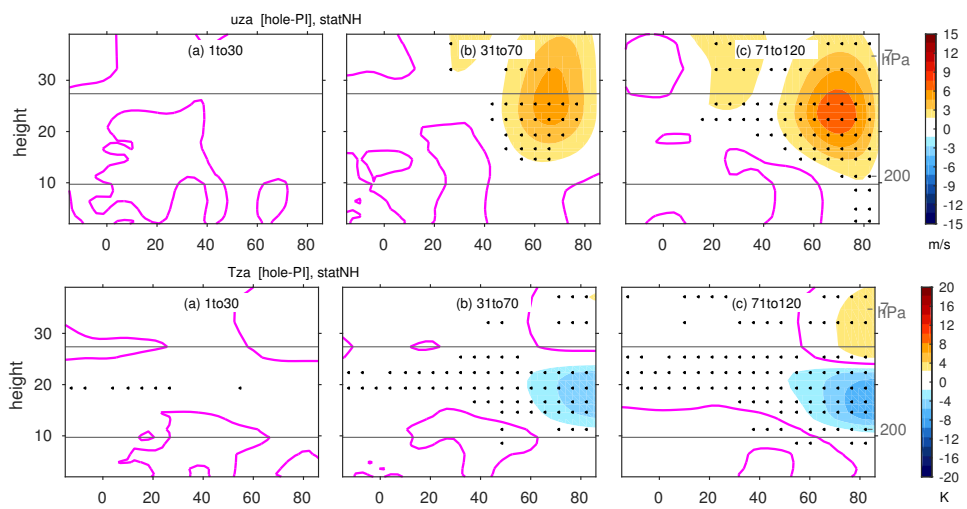


FIG. 2. Zonal-mean responses for NH ozone hole.